

NUMERICAL SOLUTION OF THE SPECTRAL PROBLEM FOR ARBITRARY SELF-ADJOINT EXTENSIONS OF THE SCHRÖDINGER EQUATION ON MANIFOLDS WITH BOUNDARY*

A. LÓPEZ-YELA[†] AND J.M. PÉREZ-PARDO[‡]

Abstract. A numerical scheme to compute a large class of self-adjoint extensions of the Laplace-Beltrami operator on manifolds with boundary in any dimension is presented. The algorithm is based on the characterisation, recently obtained by the authors, of a large class of self-adjoint extensions of Laplace-Beltrami operators in terms of their associated quadratic forms. Such extensions are determined by a unitary operator U defined on the space of data at the boundary and possessing a gap property at the eigenvalue -1 . The convergence of the scheme is proved by applying an iterated min-max argument to a specific finite elements approximation of the domain of the corresponding quadratic form that depends on the choice of the unitary map U .

An algorithm for dimension 2 is implemented effectively. It is needed a suitable approximation of the unitary operators acting on the infinite-dimensional space of data of the boundary. This is in contrast with the one-dimensional situation explored by the authors already [18], where the space of boundary data is finite-dimensional. As a consequence of the implementation of the boundary conditions in terms of a unitary operator, the numerical scheme proposed is able to treat essential and natural boundary conditions in a unified way.

Several numerical experiments are computed, showing that the algorithm is able to treat a wide variety of boundary conditions including, for instance, quasi-periodic boundary conditions (also called Bloch-periodic) or mixed type boundary conditions. As in the one-dimensional situation, the experiments confirm the existence of self-adjoint extensions where the lower eigenvalues are localised near the boundary. Such localised states play an important role in condensed state physics like Quantum Hall effect or topological insulators.

1. Introduction. The study of self-adjoint extensions of symmetric operators plays a fundamental role not only in the foundations, but increasingly so in the applications of Quantum Mechanics as they determine the spectrum of the corresponding system. Among them, it is paramount the role played by the Laplace-Beltrami operator, as it corresponds to the kinetical term of the Schrödinger equation for a quantum system of mechanical type. In the presence of boundaries, such operator is usually defined on a domain on which it is merely symmetric, but not self-adjoint. To completely determine the quantum mechanical properties of the system, boundary conditions should be imposed in such a way that the corresponding extension is self-adjoint with a real spectrum (see for instance the recent review [4] and references therein).

In dimension higher than one, it is well-known that the space of such self-adjoint extensions is infinite-dimensional. A large class of these self-adjoint extensions is described in terms of unitary operators defined on a Hilbert space of boundary data satisfying a gap property on its own spectrum around the eigenvalue -1 (see [16] and references therein). In dimension one, the problem of characterising self-adjoint extensions in such a way that their spectrum and eigenvectors can be computed efficiently was satisfactorily addressed in [18]. It was shown there that a numerical algorithm based on the finite element method (FEM), where the boundary elements were carefully crafted for the conditions imposed by the unitary operator U at the boundary, satisfied the correct properties of convergence and stability. Moreover, the algorithm was implemented and used to compute the spectrum and eigenvectors of different self-adjoint extensions. However, the algorithm proposed in [18] cannot be applied in dimension higher than one in a straightforward way. The main reason for this is that in dimension one the unitary operator describing the boundary conditions is finite-dimensional and the boundary conditions can be implemented exactly. This is not the case in dimension higher than one where in general one needs also to approximate the boundary condition. Moreover, the proof of the convergence given there was adapted to the one-dimensional setting and it does not extend to higher dimensions.

The numerical study of self-adjoint extensions for the Laplace-Beltrami operator in dimension higher than one is not only interesting from a mathematical perspective, as it involves finite

*The authors would like to give special thanks to Prof. A. Ibort for his valuable comments and useful discussions. They also acknowledge the partial support by the Spanish MINECO grant MTM2014-54692-P and QUITEMAD+, S2013/ICE-2801. A. L-Y. has been partially supported by UCIIM predoctoral Grant.

[†]Depto. de Matemáticas, Univ. Carlos III de Madrid, Avda. de la Universidad 30, 28911 Leganés, Madrid, Spain.

[‡]Sezione INFN di Napoli, Complesso Universitario di Monte S. Angelo, via Cintia, 80126 Naples, Italy.

element methods that use completely different constructions of boundary elements to the already well developed Dirichlet and Neumann boundary conditions, or more specifically, essential and natural boundary conditions, cf. [6, 10, 23]. Recent proposals like [17] require new computational tools dealing with self-adjoint extensions of Laplace-like operators to extend its applicability to actual physical systems.

In this context, boundary conditions are going to be treated as the only input parameter of the problem and the geometry will remain fixed. In the standard FEM approach, one needs to distinguish *a priori* which boundary conditions are essential and which ones are natural in order to construct the appropriate FEM. In contrast, the algorithm presented here treats natural and essential boundary conditions in a unified way. It is able to deal with a diversity of boundary conditions like Dirichlet, Neumann, Robin, mixed, periodic, quasi-periodic (also called Bloch-periodic, cf. [28] and references therein), or even more general ones like those appearing in [15] by just modifying the input parameters.

This article focuses on the construction and analysis of the aforementioned algorithm to show its capabilities. Moreover, the convergence conditions of this approach are proven not only for the particular realisation presented here, but for a general situation. The approach for the construction of finite elements at the boundary, as it is proposed here, should be taken as a complement to already existent and well-established all-purpose routines, for instance, the one presented in [27]. However, standard approaches do not allow to solve the problem for the variety of boundary conditions that can be handled with the present scheme. Implementation of more efficient approaches to speed up convergence will be considered in the future. These include mesh refinements or increasing the polynomial degree of the finite elements, i.e. implementation of h-method or p-method, as well as other recent developments like including probabilistic indetermination of the input data as it is done in [5, 8, 9]. These latter considerations will play a relevant role when considering more complex geometries than the ones considered here.

The implementation of the FEM to cope with boundary conditions defined by unitary operators at the boundary is performed by adding a rim of boundary elements to the domain that serve to implement the finite dimensional approximation of the domain of the given operator. Such elements have a particular structure that has been carefully crafted to guarantee the convergence of the domains and the quadratic forms approximating the original problem. The boundary element model, that now has a square shape, is carefully described in Section 4 as well as the matrix manipulations needed to cope with it.

Finally, a number of numerical experiments aimed to test the computational qualities as well as the potential capabilities of the algorithm are presented. First, as a way of calibrating the algorithm, the spectrum and eigenfunctions of some simple extensions, like those corresponding to periodic or Robin boundary conditions are computed and compared with the exact solutions. Self-adjoint extensions corresponding to more delicate situations, like quasi-periodic or discontinuous Robin boundary conditions are treated too. In all the cases, the correspondence with the theoretical results is showed.

2. Self-adjoint extensions of the Laplace-Beltrami operator and unitary operators at the boundary. In this section we introduce the family of operators that will be addressed by the numerical algorithm. We will present the most important results in order to keep the article as self-contained as possible. This will also serve to fix the notation.

Let $(\Omega, \partial\Omega, \eta)$ be a smooth orientable Riemannian manifold with metric η and smooth compact boundary $\partial\Omega$. We will denote as $\mathcal{C}^\infty(\Omega)$ the space of smooth functions on the Riemannian manifold Ω , and by $\mathcal{C}_c^\infty(\Omega)$ the space of smooth functions with compact support in the interior of Ω . The Riemannian volume form is denoted by $d\mu_\eta$.

The **Laplace-Beltrami Operator** associated to the Riemannian manifold $(\Omega, \partial\Omega, \eta)$ is the second order differential operator $\Delta_\eta : \mathcal{C}^\infty(\Omega) \rightarrow \mathcal{C}^\infty(\Omega)$ given in local coordinates (x^i) on Ω by

$$\Delta_\eta \Phi = \sum_{i,j} \frac{1}{\sqrt{|\eta|}} \frac{\partial}{\partial x^i} \sqrt{|\eta|} \eta^{ij} \frac{\partial \Phi}{\partial x^j}.$$

The different self-adjoint extensions of this operator describe the dynamics of a quantum free

particle moving on the manifold Ω . The Laplace-Beltrami operator can be defined in the domain consisting of smooth functions $\mathcal{C}^\infty(\Omega)$ on Ω , but it is not self-adjoint on it (neither symmetric). If the domain is restricted to the subspace $\mathcal{C}_c^\infty(\Omega)$, the operator is symmetric but not self-adjoint. It is not obvious, in fact it is a difficult problem, how to choose the domains appropriately in such a way to make the operator (essentially) self-adjoint. Moreover, once this is done, it becomes a problem to compute efficiently its spectrum.

In what follows, we describe a class of weak problems that are associated to a large family of self-adjoint extensions of the Laplace-Beltrami operator. This class contains all the well-known boundary conditions that lead to self-adjoint extensions of the Laplace-Beltrami operator like Dirichlet, Neumann or periodic boundary conditions. Furthermore, this class allows to numerically approximate its spectrum, as is showed in Section 3.

The **Sobolev space of order k** on the manifold Ω will be denoted by $\mathcal{H}^k(\Omega)$ and the associated norm and scalar product by $\|\cdot\|_k$ and $\langle \cdot, \cdot \rangle_k$ respectively. When the manifold to be considered is not clear from the context, we will use the more explicit subindices $\|\cdot\|_{\mathcal{H}^k(\Omega)}$ and $\langle \cdot, \cdot \rangle_{\mathcal{H}^k(\Omega)}$. The boundary of the Riemannian manifold is going to be denoted by $\partial\Omega$ and the Riemannian measures, on the manifold Ω and its boundary $\partial\Omega$, by μ_Ω and $\mu_{\partial\Omega}$ respectively. The spaces of smooth functions over the two manifolds verify that $\mathcal{C}^\infty(\Omega)|_{\partial\Omega} \simeq \mathcal{C}^\infty(\partial\Omega)$. There is an important relation between the Sobolev spaces defined over the manifolds Ω and $\partial\Omega$. This is the well-known Lions' trace theorem (cf. [2, Theorem 7.39], [21, Theorem 8.3]) which we particularise for $\mathcal{H}^1(\Omega)$:

THEOREM 2.1 (Lions' trace theorem). *Let $\Phi \in \mathcal{C}^\infty(\Omega)$ and let $\gamma : \mathcal{C}^\infty(\Omega) \rightarrow \mathcal{C}^\infty(\partial\Omega)$ be the trace map $\gamma(\Phi) = \Phi|_{\partial\Omega}$. There is a unique continuous extension of the trace map such that:*

- i) $\gamma : \mathcal{H}^1(\Omega) \rightarrow \mathcal{H}^{1/2}(\partial\Omega)$.
- ii) *The map is surjective .*

The result above shows that $\mathcal{H}_0^1 := \ker\gamma$ is a closed subspace of $\mathcal{H}^1(\Omega)$. Accordingly, we can introduce the following decomposition.

DEFINITION 2.2. *Let \mathcal{H}_b denote the orthogonal complement of $\mathcal{H}_0^1 := \ker\gamma$ with respect to the scalar product in \mathcal{H}^1 . We shall call it the **boundary Sobolev space**. The orthogonal projections onto these closed subspaces shall be denoted by π_b and π_0 respectively.*

The following result shall be useful later on.

COROLLARY 2.3. *The restriction of the trace map to the boundary Sobolev space defines a continuous bijection:*

$$\gamma_b : \mathcal{H}_b \rightarrow \mathcal{H}^{1/2} .$$

Proof. Continuity is an immediate consequence of Lions' trace theorem. Moreover, since \mathcal{H}_b and $\ker\gamma$ are orthogonal, we have that

$$\ker\gamma|_{\mathcal{H}_b} = \mathcal{H}_b \cap \ker\gamma = 0 .$$

Since γ is surjective for all $\varphi \in \mathcal{H}^{1/2}$ there exists $\Phi \in \mathcal{H}^1$ such that $\varphi = \gamma(\Phi)$ and we have that

$$\varphi = \gamma(\Phi) = \gamma(\pi_b\Phi + \pi_0\Phi) = \gamma(\pi_b\Phi) = \gamma_b\pi_b\Phi ,$$

where $\pi_0\Phi \in \ker\gamma$ and $\pi_b\Phi \in \mathcal{H}_b$. \square

In order to prove the convergence results we will use the well-known notion of closed, semi-bounded quadratic forms and their relation with self-adjoint operators. These provide the appropriate analytic setting for our purposes. Standard references on this subject are [20, Chapter VI], [24, Section VIII.6] or [12, Section 4.4].

We recall here some results from [16] that describe a large class of self-adjoint extensions of the Laplace-Beltrami operator obtained via the representation theorem of closed semibounded quadratic forms, cf. [24, Thm. VIII.15]. The extensions are parameterized in terms of suitable unitary operators on the Hilbert space of square integrable functions on the boundary. Before introducing this family, we shall need some definitions.

DEFINITION 2.4. *Let U be unitary and denote its spectrum by $\sigma(U)$. The unitary operator U has **spectral gap at -1** if one of the following conditions hold:*

- i) $\mathbb{I} + U$ is invertible.
- ii) $-1 \in \sigma(U)$ and -1 is not an accumulation point of $\sigma(U)$.

*The eigenspace associated to the eigenvalue -1 is denoted by W and called the **relevant subspace**. The corresponding orthogonal projections will be written as P_U and $P_U^\perp = \mathbb{I} - P_U$.*

DEFINITION 2.5. *Let U be a unitary operator with spectral gap at -1 . The **partial Cayley transform** $A_U: \mathcal{L}^2(\partial\Omega) \rightarrow \mathcal{L}^2(\partial\Omega)$ is the bounded operator*

$$A_U := iP_U^\perp(U - \mathbb{I})(U + \mathbb{I})^{-1}.$$

DEFINITION 2.6. *Let $U: \mathcal{L}^2(\partial\Omega) \rightarrow \mathcal{L}^2(\partial\Omega)$ be a unitary operator with spectral gap at -1 . The unitary is said to be **admissible** if the partial Cayley transform A_U leaves the subspace $\mathcal{H}^{1/2}(\partial\Omega)$ invariant and is continuous with respect to the Sobolev norm of order $1/2$, i.e. there exists $K \in \mathbb{R}$ such that*

$$\|A_U\varphi\|_{\mathcal{H}^{1/2}(\partial\Omega)} \leq K\|\varphi\|_{\mathcal{H}^{1/2}(\partial\Omega)}, \quad \forall \varphi \in \mathcal{H}^{1/2}(\partial\Omega).$$

DEFINITION 2.7. *Let $U: \mathcal{L}^2(\partial\Omega) \rightarrow \mathcal{L}^2(\partial\Omega)$ be a unitary operator with spectral gap at -1 . The domain \mathcal{D}_U associated to the unitary operator $U \in \mathcal{U}(\mathcal{L}^2(\partial\Omega))$ with gap at -1 is defined by*

$$\mathcal{D}_U = \{\Phi \in \mathcal{H}^1(\Omega) \mid P_U\gamma(\Phi) = 0\}. \quad (2.1)$$

DEFINITION 2.8. *Let $U: \mathcal{L}^2(\partial\Omega) \rightarrow \mathcal{L}^2(\partial\Omega)$ be a unitary operator with spectral gap at -1 , A_U the corresponding partial Cayley transform and γ the trace map considered in Thm. 2.1. The Hermitean quadratic form Q_U with domain \mathcal{D}_U is defined by*

$$Q_U(\Phi, \Psi) = \langle d\Phi, d\Psi \rangle - \langle \gamma(\Phi), A_U\gamma(\Psi) \rangle_{\partial\Omega}.$$

It is worth to mention the reasons behind Def. 2.4 and Def. 2.6. The spectral gap condition ensures that the partial Cayley transform becomes a bounded self-adjoint operator on the subspace W^\perp and this is enough to guarantee that the quadratic form Q_U is lower semi-bounded, cf. [16]. The admissibility condition is an analytic requirement to ensure that Q_U is a closable quadratic form. As a remark, let us say that the splitting of the unitary operator U into the proper subspace associated to $\{-1\}$ and the partial Cayley transform A_U can be understood as an analytical manifestation of the difference between essential and natural boundary conditions.

The next theorem characterises the class of self-adjoint extensions of the minimal Laplace-Beltrami operator $-\Delta_{\min}$ that we will be interested in. We refer to [16] for a complete proof and additional motivation.

THEOREM 2.9. *Let $U: \mathcal{L}^2(\partial\Omega) \rightarrow \mathcal{L}^2(\partial\Omega)$ be an admissible unitary operator with spectral gap at -1 . Then, the quadratic form Q_U with domain \mathcal{D}_U is semi-bounded from below and closable. Its closure is represented by a semi-bounded self-adjoint extension of the minimal Laplacian $-\Delta_{\min}$. We shall denote this self-adjoint extension by $-\Delta_U$.*

The relation between the unitary operator U and the self-adjoint operator $-\Delta_U$ can be summarised as follows. The self-adjoint operator $-\Delta_U$ is the self-adjoint extension of the minimal Laplace-Beltrami operator that satisfies the boundary condition

$$\varphi - i\dot{\varphi} = U(\varphi + i\dot{\varphi}) . \quad (2.2)$$

Here, $\varphi = \gamma(\Phi)$ and $\dot{\varphi} = \gamma\left(\frac{d\Phi}{dn}\right)$, i.e. the restriction to the boundary of the function Φ and its normal derivative respectively. The normal direction is taken pointing outwards the manifold. More specifically, $-\Delta_U$ is the self-adjoint extension with domain

$$\mathcal{D}(\Delta_U) = \{\Phi \in \mathcal{H}^2(\Omega) \mid \varphi - i\dot{\varphi} = U(\varphi + i\dot{\varphi})\} . \quad (2.3)$$

3. Approximations of the spectral problem in arbitrary dimension by finite element methods. In this section we develop a class of numerical algorithms, based in the finite element method, that can be used to approximate the spectral problem for the self-adjoint extensions of the Laplace-Beltrami operator described in Section 2. A standard reference for this method is [11].

In what follows, let $-\Delta_U$ denote the self-adjoint operator associated to the closure of the quadratic form Q_U of Def. 2.8. Thm. 2.9 ensures that this closure exists and that the operator $-\Delta_U$, with domain $\mathcal{D}(\Delta_U)$, is semi-bounded from below. Moreover, $-\Delta_U$ is a self-adjoint extension of $-\Delta_{\min}$.

We are interested in obtaining numerical approximations of pairs $(\Phi, \lambda) \in \mathcal{L}^2(\Omega) \times \mathbb{R}$ that are solutions of the spectral problem

$$-\Delta_U \Phi = \lambda \Phi \quad \Phi \in \mathcal{D}(\Delta_U) . \quad (3.1)$$

As usual in finite element methods, the solutions can be obtained by approximating the solution of the problem in the weak form. That is, a pair $(\Phi, \lambda) \in \mathcal{L}^2(\Omega) \times \mathbb{R}$ is a solution of the spectral problem (3.1) if and only if it is a solution of the weak spectral problem

$$Q_U(\Psi, \Phi) = \lambda \langle \Psi, \Phi \rangle \quad \forall \Psi \in \mathcal{D}_U , \quad (3.2)$$

with \mathcal{D}_U the domain of the quadratic form Q_U given in Eq. (2.1). Proving this equivalence is straightforward using the definitions of the previous section.

The way we shall approximate the solution of the weak spectral problem (3.2) is by finding a family of finite-dimensional problems, in terms of an appropriate family of finite-dimensional spaces $\{S_U^N\}$, that verifies approximately the boundary conditions. Then, we will look for solutions $(\Phi_N, \lambda_N) \in S_U^N \times \mathbb{R}$ of these approximate spectral problems. Since the boundary conditions, represented by the unitary operator U , will also be approximated, we need to look for solutions of a finite-dimensional problem of the form

$$Q_{U^N}(\Psi_N, \Phi_N) = \lambda_N \langle \Psi_N, \Phi_N \rangle, \quad \forall \Psi_N \in S_U^N . \quad (3.3)$$

where $\{U^N\}$ is a family of unitary operators.

The rest of this section is devoted to obtain sufficient conditions on the family $\{S_U^N\}$ such that the solutions of the approximate spectral problem (3.3) converge to the solutions of the weak spectral problem (3.2). In Section 4, we construct explicitly a family $\{S_U^N\}$ for the two-dimensional case. Due to the non-locality of generic boundary conditions, one needs to introduce a non-local subspace of functions that is able to encode them.

Before introducing the actual algorithm, which will be done in Section 4, we discuss the general conditions guaranteeing convergence of the proposed numerical scheme. In particular, one needs to address the problem of approximating the boundary conditions. It is worth mentioning that the considerations of this section work regardless of the dimension of the underlying manifold and serve as a stepping stone for implementations in any dimension.

In what follows we assume that the unitary operator U describing the quadratic form Q_U is admissible, cf. Def. 2.6. Hence, we are under the conditions of Thm. 2.9 and therefore the quadratic form

$$Q_U(\Phi, \Psi) = \langle d\Phi, d\Psi \rangle - \langle \gamma(\Phi), A_U \gamma(\Phi) \rangle_{\partial\Omega} \quad (3.4)$$

with domain $\mathcal{D}_U = \{\Phi \in \mathcal{H}^1(\Omega) \mid P_U \gamma(\Phi) = 0\}$, where A_U is the partial Cayley transform of Def. 2.5, is closable and semi-bounded from below.

We introduce now sufficient conditions on the family of finite-dimensional problems to ensure convergence to the solutions of the aforementioned spectral problem (3.1). First of all, one needs a family of finite-dimensional subspaces that approximate the Sobolev spaces of order 1. We shall call each member of this family a **finite elements space** and denote it by S^N , where $N \in \mathbb{Z}$ denotes the vector space dimension. We denote by $\{\Pi^N\}_{N \in \mathbb{Z}}$ the family of projections onto these subspaces:

$$\Pi^N : \mathcal{H}^1(\Omega) \rightarrow S^N .$$

In general, this projections are not orthogonal projections. As a general assumption we need to impose that

$$\|(\Pi^N - \mathbb{I})\Phi\|_1 \xrightarrow{N \rightarrow \infty} 0 . \quad (3.5)$$

Since each S^N is a closed subspace of $\mathcal{H}^1(\Omega)$, one can define the traces of these subspaces as

$$s^N = \{\varphi \in \mathcal{H}^{1/2}(\partial\Omega) \mid \varphi = \gamma(\Phi), \Phi \in S^N\} . \quad (3.6)$$

We will call them **traces of the finite element spaces**. Notice that the traces of the finite element spaces do not have dimension N in general, but are also finite-dimensional subspaces with $\dim s^N \leq N$.

ASSUMPTION 1. *Let $U \in \mathcal{U}(\mathcal{L}^2(\partial\Omega))$ be an admissible unitary operator with gap. Let $\{U^N\}_{N \in \mathbb{Z}}$ be a family of unitary operators such that $U^N \in \mathcal{U}(s^N)$. The projections onto the relevant subspaces*

$$P_{U^N} : s^N \rightarrow s^N$$

and the partial Cayley transforms

$$A_{U^N} : s^N \rightarrow s^N$$

can be lifted to $\mathcal{H}^{1/2}(\partial\Omega)$ by considering that the orthogonal complement to s^N with respect to the scalar product in $\mathcal{H}^{1/2}(\partial\Omega)$ is in their kernel. Let the operators constructed this way be denoted with the same symbol respectively. We assume:

- i) $\|(P_{U^N} - P_U)\varphi\|_{\mathcal{H}^{1/2}(\partial\Omega)} \xrightarrow{N \rightarrow \infty} 0, \quad \varphi \in \mathcal{H}^{1/2} .$
- ii) $\langle \psi, (A_{U^N} - A_U)\varphi \rangle_{\mathcal{L}^2(\partial\Omega)} \xrightarrow{N \rightarrow \infty} 0 .$

DEFINITION 3.1. *Let $\{U^N\}_N$ be a family of unitary operators satisfying Assumption 1. Consider the finite-dimensional subspaces*

$$S_U^N = \{\Phi \in S^N \mid P_{U^N} \gamma(\Phi) = 0\} . \quad (3.7)$$

*The family $\{S_U^N\}_N$ will be called an **approximating family** of the spectral problem (3.1).*

We prove the convergence in two steps. First, we shall prove the convergence of the eigenvalues. After that we will be able to prove the convergence of the eigenfunctions.

LEMMA 3.2. *Let $\{S_U^N\}_N$ be an approximating family and let $\{\lambda^N\}_N$ be the sequence of eigenvalues corresponding to the n -th lowest eigenvalue of the approximate spectral problem (3.3). This sequence converges to the n -th lowest eigenvalue of the weak spectral problem (3.2).*

Proof. Let V_n and V_n^N be the spaces

$$V_n = \{ \Phi \in \mathcal{D}_U \mid \langle \Phi, \xi_i \rangle = 0, \xi_i \in \mathcal{L}^2(\Omega), i = 1, \dots, n \}, \quad (3.8)$$

$$V_n^N = \{ \Phi_N \in S_U^N \mid \langle \Phi_N, \xi_i \rangle = 0, \xi_i \in \mathcal{L}^2(\Omega), i = 1, \dots, n \}. \quad (3.9)$$

Then, applying the min-max Principle, cf. [25, Thm. XIII.2], to the quadratic form Q_U of Def. 2.8 on the domains of the weak and the approximate spectral problems, and subtracting them, we get:

$$\sup_{\xi_1, \dots, \xi_{n-1}} \left[\inf_{\Phi_N \in V_{n-1}^N} \frac{Q_U(\Phi_N)}{\|\Phi_N\|^2} - \inf_{\Phi \in V_{n-1}} \frac{Q_U(\Phi)}{\|\Phi\|^2} \right] = \widetilde{\lambda}^N - \lambda. \quad (3.10)$$

Where $\widetilde{\lambda}^N$ is the n -th eigenvalue of the finite-dimensional problem defined by the quadratic form Q_U with domain S_U^N and λ is the n -th eigenvalue of the weak spectral problem. Notice that $\widetilde{\lambda}^N$ is not an eigenvalue of the approximate problem (3.3) since for the moment we are considering only the quadratic form Q_U and not Q_{U^N} . Let $\|\cdot\|^2 := Q_U(\cdot) + (m+1)\|\cdot\|^2$ be the graph-norm of the quadratic form Q_U , where m is its lower bound, cf. Thm. 2.9. By adding and subtracting $(m+1)\|\Phi\|^2$, forgetting the supremum for the moment, and considering that all the functions are normalised in $\mathcal{L}^2(\Omega)$, we get that the left hand side of Eq. (3.10) verifies for $\Phi \in V_{n-1} \subset \mathcal{D}_U$:

$$\inf_{\Phi_N \in V_{n-1}^N} \|\Phi_N\|^2 - \inf_{\tilde{\Phi} \in V_{n-1}} \|\tilde{\Phi}\|^2 \leq \|\Phi\|^2 - \inf_{\tilde{\Phi} \in V_{n-1}} \|\tilde{\Phi}\|^2 + \inf_{\Phi_N \in V_{n-1}^N} (\|\Phi - \Phi_N\|^2 + 2\|\Phi\|\|\Phi - \Phi_N\|), \quad (3.11)$$

Now, for all $\epsilon > 0$ we can select $\Phi \in V_{n-1}$ such that

$$\left| \|\Phi\|^2 - \inf_{\tilde{\Phi} \in V_{n-1}} \|\tilde{\Phi}\|^2 \right| < \epsilon.$$

Therefore,

$$\inf_{\Phi_N \in V_{n-1}^N} \|\Phi_N\|^2 - \inf_{\tilde{\Phi} \in V_{n-1}} \|\tilde{\Phi}\|^2 \leq \epsilon + \inf_{\Phi_N \in V_{n-1}^N} (\|\Phi - \Phi_N\|^2 + 2\|\Phi\|\|\Phi - \Phi_N\|). \quad (3.12)$$

Since the graph norm of the quadratic form is dominated by the Sobolev norm $\|\cdot\|_1$, in order to bound the right hand side it is enough to show that for a fixed $\Phi \in \mathcal{D}_U$

$$\inf_{\Phi_N \in S_U^N} \|\Phi - \Phi_N\|_1 \xrightarrow{N \rightarrow \infty} 0.$$

From Eq. (3.5), there exists for every $\Phi \in \mathcal{D}_U \subset \mathcal{H}^1$ and every $\epsilon > 0$ an N_0 such that for all $N > N_0$ we have that

$$\|\Phi - \Pi^N \Phi\|_1^2 \leq \epsilon. \quad (3.13)$$

Notice that $\Pi^N \Phi$ is not an element of S_U^N in general. Using the decomposition of Def. 2.2 and Cor. 2.3 we can define

$$\widetilde{\Phi}^N := \gamma_b^{-1}(\mathbb{I} - P_{U^N})\gamma_b\pi_b\Pi^N\Phi + \pi_0\Pi^N\Phi.$$

It is easy to check that $\widetilde{\Phi}^N \in S_U^N$. Now, we get:

$$\begin{aligned} \|\Phi - \widetilde{\Phi}^N\|_1^2 &= \|\pi_0\Phi - \pi_0\widetilde{\Phi}^N\|_1^2 + \|\pi_b\gamma_b^{-1}(\mathbb{I} - P_{U^N})\gamma_b\pi_b\Pi^N\Phi - \pi_b\Phi\|_1^2 \\ &\leq \|\pi_0(\mathbb{I} - \Pi^N)\Phi\|_1^2 + K\|(\mathbb{I} - P_{U^N})\gamma_b\pi_b\Pi^N\Phi - \gamma(\pi_b\Phi)\|_{\mathcal{H}^{1/2}(\partial\Omega)}^2 \\ &\leq \|\pi_0(\mathbb{I} - \Pi^N)\Phi\|_1^2 + K\|(\mathbb{I} - P_{U^N})(\gamma_b\pi_b\Pi^N\Phi - \gamma_b\pi_b\Phi)\|_{\mathcal{H}^{1/2}(\partial\Omega)}^2 \\ &\quad + K\|(P_{U^N} - P_U)\gamma_b\pi_b\Phi\|_{\mathcal{H}^{1/2}(\partial\Omega)}^2, \end{aligned}$$

where K is the Lipschitz constant of the bijection γ_b . The right hand side can be chosen as small as needed by means of Eq. (3.13) and Assumption 1. Similar arguments lead to a similar bound for the reverse difference in Eq. (3.10), and hence we have proved that

$$|\widetilde{\lambda}_N - \lambda| \rightarrow 0.$$

Finally, we need to show that the n -th eigenvalue of the finite-dimensional problems Q_U and Q_{U^N} , both with domain S_U^N converge, i.e. $|\lambda_N - \widetilde{\lambda}_N| \rightarrow 0$. We shall use the min-max principle again. Notice that

$$\frac{Q_U(\Phi)}{\|\Phi\|^2} - \frac{Q_{U^N}(\Phi)}{\|\Phi\|^2} = -\frac{\langle \varphi, (A_U - A_{U^N})\varphi \rangle}{\|\Phi\|^2} \leq K \|A_U - A_{U^N}\|_{L(S_U^N)} \frac{\|\Phi\|_1^2}{\|\Phi\|^2}. \quad (3.14)$$

If we apply the min-max Principle to both sides, we get that

$$|\widetilde{\lambda}_N - \lambda_N| \leq K' \|A_U - A_{U^N}\|_{L(S_U^N)} \sup_{\xi_1, \dots, \xi_{n-1}} \inf_{\Phi_N \in V_{n-1}^N} \frac{\|\Phi\|_1^2}{\|\Phi\|^2}. \quad (3.15)$$

Now notice that $\|\Phi\|_1^2$ is proportional to the quadratic form associated to the Dirichlet extension of the Laplace-Beltrami operator. Since $S_{\text{Dirichlet}}^N \subset S_U^N$, we have that

$$\sup_{\xi_1, \dots, \xi_{n-1}} \inf_{\Phi_N \in V_{n-1}^N} \frac{\|\Phi\|_1^2}{\|\Phi\|^2} \leq K(\lambda^D + 1),$$

where λ^D is the n -th eigenvalue of the Dirichlet extension of the Laplace-Beltrami operator on the manifold Ω . Finally, notice that the factor $\|A_U - A_{U^N}\|_{L(S_U^N)}$ is the operator norm over a finite-dimensional subspace of $\mathcal{L}^2(\partial\Omega)$. Hence, the weak convergence condition in Assumption 1 guarantees that the right hand side of Eq. (3.15) can be chosen as small as needed. \square

LEMMA 3.3. *Let $\{S_U^N\}_N$ be an approximating family and let $\{\Phi^N\}_N$ be a sequence of eigenfunctions associated to the sequence $\{\lambda_N\}_N$ of Lemma 3.2. Let $\|\cdot\|$ be the graph norm of the quadratic form Q_U . Then, by passing to a subsequence if necessary, there exists $\Phi \in \overline{\mathcal{D}_U^{\|\cdot\|}}$ such that for any $\Psi \in \overline{\mathcal{D}_U^{\|\cdot\|}}$*

$$Q_U(\Psi, \Phi - \Phi^N) \xrightarrow{N \rightarrow \infty} 0,$$

and such that for all $\Psi \in \overline{\mathcal{D}_U^{\|\cdot\|}}$

$$Q(\Psi, \Phi) = \lambda \langle \Psi, \Phi \rangle.$$

Proof. We can assume that $\|\Phi^N\|_1 = 1$. By Banach-Alaoglu theorem and the fact that the Sobolev norm of order 1 dominates the graph-norm of the quadratic form, there exist subsequences $\{\Phi^{N_j}\}$ and accumulations points Φ such that for any $\Psi \in \overline{\mathcal{D}_U^{\|\cdot\|}}$ it holds that

$$Q_U(\Psi, \Phi - \Phi_j^N) \xrightarrow{N_j \rightarrow \infty} 0.$$

Proving that Φ is a solution of the weak eigenvalue problem is a straightforward calculation using that weak convergence in $\overline{\mathcal{D}_U^{\|\cdot\|}}$ implies weak convergence in $\mathcal{L}^2(\Omega)$, that $|\lambda_N - \lambda| \rightarrow 0$ and that

$$|Q_U(\Psi, \Phi) - Q_{U^N}(\Psi, \Phi)| \leq K |\langle \psi, (A_U - A_{U^N})\varphi \rangle|,$$

whose right hand side tends to zero by Assumption 1. \square

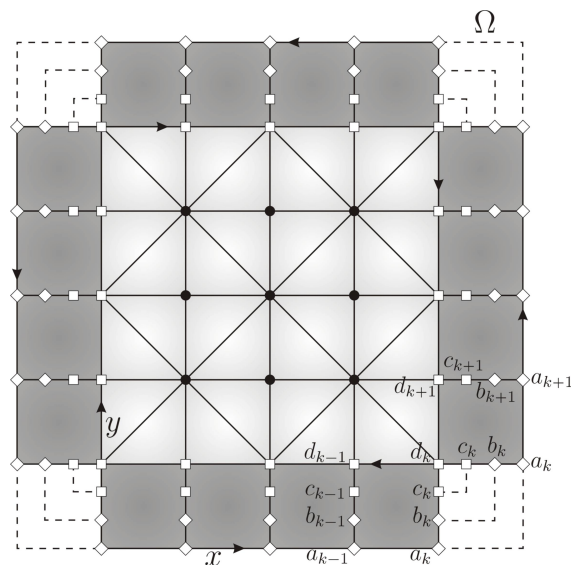


Fig. 4.1: Triangularisation of the problem for $n = m = 5$. White region corresponds to the triangularised part at the bulk and the dark squares to the boundary. Regularisation at the corners is achieved by identification of the nodes at each corner. Bulk nodes are depicted in black. There are two types of nodes at the finite elements of the boundary. The interior nodes are problem nodes and are denoted with squares. The exterior nodes, called *boundary nodes* are depicted with rhombi.

4. Finite element method approximation of the spectral problem. The finite element model that we shall use has to be devised in order to satisfy Eq. (3.5). Well known results in finite elements theory establish that piecewise linear continuous functions satisfy the convergence condition of Eq. (3.13) discussed in the previous section, cf. [11]. The construction of the algorithm will be split into two main parts, one considering the construction of the finite elements at the bulk, and other considering the finite elements at the boundary.

As the region Ω we consider the square $[0, 1] \times [0, 1]$ with the triangularisation given in Fig. 4.1. The factors n and m correspond to the number of node points in which the grid is divided, where n denotes the number of nodes on the horizontal axis and m the number of nodes on the vertical one, (for simplicity we will consider them equal, i.e. $n = m$).

Let us remark that at the bulk we have divided the squares in two right triangles. There, we will apply a standard FEM where the base-functions have value one at one node and zero at the rest. At the boundary, the finite elements will be squares and the base-functions will depend on the boundary conditions of the problem under consideration. The reason behind the choice of square elements at the boundary will become clear when dealing with the construction of the finite element models at the boundary. The regularisation procedure that we consider at the corners of the manifold Ω is the identification of the sides of the squares at the corners as shown in Fig. 4.1. This way we implicitly solve the ill-definedness problem of the normal derivatives at the corners.

Let us reformulate the problem of Def. 2.8 as it is usually done in FEM. First, we write the solution function Φ and the function Ψ in terms of base-functions:

$$\Phi = \sum_{i=1}^N u_i \phi_i, \quad \Psi = \sum_{i=1}^N v_i \phi_i, \quad (4.1)$$

where N is the total number of base-functions. Hence, (3.3) becomes:

$$\sum_{i,j=1}^N [u_i (M_{ij} - F_{ij}) v_j] = \lambda \sum_{i,j=1}^N u_i B_{ij} v_j, \quad \forall v_j, \quad (4.2)$$

where the matrices M , B and F are defined as:

$$M_{ij} = \int_{\Omega} (\phi_{ix}\phi_{jx} + \phi_{iy}\phi_{jy}) d\mu_{\eta}, \quad B_{ij} = \int_{\Omega} \phi_i\phi_j d\mu_{\eta}, \quad (4.3a)$$

and

$$F_{ij} = \int_{\partial\Omega} (\phi_{ix}n_1 + \phi_{iy}n_2) \phi_j d\mu_{\partial\eta}, \quad (4.3b)$$

where the subindexes x and y denote the partial derivatives with respect to x and y respectively, and $\mathbf{n} = (n_1, n_2)$ is the normal vector to the boundary. We are going to treat essential and natural boundary conditions in a unified way. Therefore, the matrix F represents the boundary term $\langle \varphi, \dot{\varphi} \rangle_{\partial\Omega}$ coming from the integration by parts formula. We explain the reasons behind this choice in Section 4.2. The problem that we solve numerically becomes then:

$$(M - F)\mathbf{u} = \lambda B\mathbf{u}, \quad (4.4)$$

with $\mathbf{u} = (u_1, u_2, \dots, u_N)$.

4.1. Finite elements at the bulk. The most relevant part of the algorithm corresponds to the boundary conditions that will be encoded in the base-functions at the boundary. The structure of the triangularisation in Fig. 4.1 makes it simple to compute the contributions of the finite elements at the bulk. As we are interested in showing the performance of the algorithm based on the boundary elements, we will consider just linear base-functions ϕ_i , $i = 1, \dots, N_{Bulk}$ at the bulk, leaving higher order finite elements for future implementations. The base-function corresponding to the i -th node has value 1 in that node and zero at the rest:

$$\phi_i(\text{node}_j) = \begin{cases} 1 & i = j \\ 0 & i \neq j \end{cases}. \quad (4.5)$$

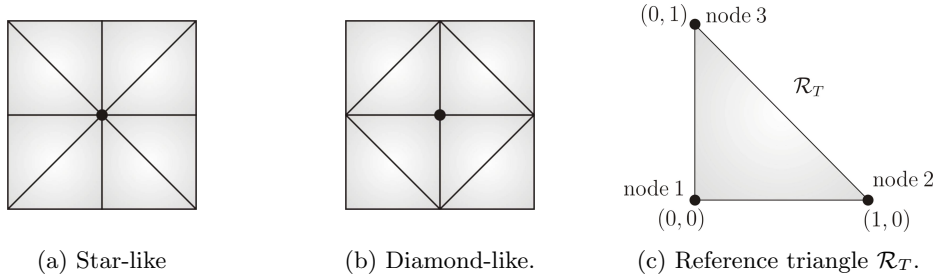


Fig. 4.2: The two different kind of nodes of the bulk and the reference triangle.

In Fig. 4.1, it can be seen that there are two kind of nodes at the bulk, the star-like and the diamond-like. Those are depicted respectively in Fig. 4.2a and Fig. 4.2b. Having this into account, it is easy to compute the matrix elements of M and B corresponding to the bulk. We have chosen the reference triangle with coordinates (η, ξ) showed in Fig. 4.2c. The affine transformation that transforms the reference triangle \mathcal{R}_T in any triangle with vertices (x_1, y_1) , (x_2, y_2) and (x_3, y_3) is the following:

$$\begin{pmatrix} x \\ y \end{pmatrix} = \begin{pmatrix} x_1 \\ y_1 \end{pmatrix} + \begin{pmatrix} x_2 - x_1 & x_3 - x_1 \\ y_2 - y_1 & y_3 - y_1 \end{pmatrix} \begin{pmatrix} \eta \\ \xi \end{pmatrix}. \quad (4.6)$$

Hence, the elements of the first derivatives of the coordinates in the reference triangle with respect to x and y are given by:

$$\begin{pmatrix} \eta_x & \eta_y \\ \xi_x & \xi_y \end{pmatrix} = \frac{1}{J_T} \begin{pmatrix} y_3 - y_1 & x_1 - x_3 \\ y_1 - y_2 & x_2 - x_1 \end{pmatrix}, \quad (4.7)$$

where the Jacobian is given by $J_T = |(x_2 - x_1)(y_3 - y_1) - (x_1 - x_3)(y_1 - y_2)|$. Let us denote by $(\alpha_i, \beta_i, \gamma_i)$ the coefficients of the base-function ϕ_i restricted to a given triangle, that is

$$\phi_i|_T = \alpha_i + \beta_i x + \gamma_i y. \quad (4.8)$$

Then, the results of the integrals (4.3a) of the matrix elements of M and B , corresponding to any triangle in our triangularisation, cf. Fig. 4.1, are:

$$M_{ij}|_T = \frac{J_T}{2} [(\beta_i \eta_x + \gamma_i \xi_x)(\beta_j \eta_x + \gamma_j \xi_x) + (\beta_i \eta_y + \gamma_i \xi_y)(\beta_j \eta_y + \gamma_j \xi_y)]|_T, \quad (4.9a)$$

$$B_{ij}|_T = \frac{J_T}{2} \left[\alpha_i \alpha_j + \frac{\alpha_i \beta_j + \beta_i \alpha_j}{3} + \frac{\alpha_i \gamma_j + \gamma_i \alpha_j}{3} + \frac{\beta_i \gamma_j + \gamma_i \beta_j}{12} + \frac{\beta_i \beta_j}{6} + \frac{\gamma_i \gamma_j}{6} \right]|_T. \quad (4.9b)$$

The matrix elements of M and B are computed by adding the latter results over all the triangles in the triangularisation:

$$M_{ij} = \sum_T M_{ij}|_T, \quad B_{ij} = \sum_T B_{ij}|_T. \quad (4.10)$$

Because of the definition of the base-functions at the bulk, if $i \neq j$ the former additions restrict to the two triangles that share the edge between the nodes i and j . If $i = j$, it is obvious that the support of the integrands of M_{ii} and B_{ii} is the same as the support of the base-function located at i , hence we will have two kinds of matrix elements depending if i is a star-like or a diamond-like node. In the former case the sum will restrict to eight triangles and in the latter to four, see Fig. 4.2.

4.2. Finite elements at the boundary. As stated at the beginning of this section, piecewise linear continuous functions provide the appropriate convergence with respect to the Sobolev norms, cf. [11]. We will consider a finite element model that guarantees that the restriction to the boundary of the functions, as well as their normal derivatives, are piecewise linear continuous functions. This condition implies that the finite element model on the region at the boundary (dark region in Fig. 4.1) cannot consist on linear polynomials. This is so because the normal derivative of a piecewise linear continuous function is a piecewise constant function. Notice that going to higher order polynomials does not spoil the convergence in the Sobolev norm of the FEM as long as continuity is preserved between finite elements.

A convenient way of imposing the boundary conditions is as follows: Instead of using the operators P_{U^N} and A_{U^N} to construct the approximate problem directly, we will construct functions at the boundary that satisfy the boundary condition

$$\varphi - i\dot{\varphi} = U^N(\varphi + i\dot{\varphi}), \quad (4.11)$$

where P_{U^N} is the orthogonal projector onto the proper space of U^N associated to the eigenvalue $\{-1\}$, A_{U^N} is the partial Cayley transform of Def. 2.5, $\varphi = \gamma(\Phi)$ is the restriction of Φ to the boundary, and $\dot{\varphi} = \gamma(\frac{d\Phi}{dn})$ is the restriction of the normal derivative. Notice that Eq. (4.11) splits into two equations, one on the proper subspace of U^N associated to $\{-1\}$ and one on its orthogonal complement:

$$P_{U^N} \varphi - iP_{U^N} \dot{\varphi} = -(P_{U^N} \varphi + iP_{U^N} \dot{\varphi}) \Leftrightarrow P_{U^N} \varphi = 0, \quad (4.12a)$$

$$P_{U^N}^\perp \varphi - iP_{U^N}^\perp \dot{\varphi} = U^N|_{\text{ran} P_{U^N}^\perp} (P_{U^N}^\perp \varphi + iP_{U^N}^\perp \dot{\varphi}) \Leftrightarrow P_{U^N}^\perp \dot{\varphi} = iP_U^\perp \frac{(U - \mathbb{I})}{U + \mathbb{I}} P_{U^N}^\perp \varphi. \quad (4.12b)$$

That is, the problem defined by

$$\langle d\Phi, d\Phi \rangle - \langle \varphi, \dot{\varphi} \rangle = \lambda \langle \Phi, \Phi \rangle,$$

such that Φ verifies the boundary condition in Eq. (4.11), is equivalent to the approximate problem of Eq. (3.3). Notice that there is a one-to-one correspondence between unitary operators U^N and the operators P_{U^N} and A_{U^N} .

The finite element model that we will consider at the boundary shall be constructed in such a way that the restrictions to the boundary of the base-functions are piecewise linear continuous functions. That is, for the interval $I_j = [x_j, x_j + h]$ each boundary function will have the following restrictions to the boundary:

$$L^j(x) = \frac{1}{h}(a_{j+1} - a_j)x - \frac{1}{h}(a_{j+1} - a_j)x_j + a_j, \quad (4.13a)$$

$$\dot{L}^j(x) = \frac{1}{h}(n_{j+1} - n_j)x - \frac{1}{h}(n_{j+1} - n_j)x_j + n_j, \quad (4.13b)$$

where, for simplicity, the interval length h is assumed to be the same at all the intervals. The former function $L^j(x)$ is the restriction of the base-function to the interval I_j , where a_j and a_{j+1} are the values of the base-function at the endpoints of the interval I_j . The latter are determined by x_j and $x_{j+1} = x_j + h$ respectively. Similarly, $\dot{L}^j(x)$ is the linear function at the interval I_j corresponding to the restriction to the boundary of the normal derivative of the base-function. In this case, n_j and n_{j+1} are the values of the normal derivatives at the nodes x_j and x_{j+1} respectively.

In order to represent the unitary operator U^N , we will choose an orthonormal basis given in terms of the Legendre polynomials of order 0 and 1 defined over each interval. Assume that there are N_S different intervals at the boundary, i.e. N_S different squares, and consider the basis given by

$$P_0^j(x) = \frac{1}{\sqrt{h}}, \quad P_1^j(x) = \frac{2\sqrt{3}}{\sqrt{h^3}}(x - x_j - \frac{h}{2}), \quad x \in [x_j, x_j + h], \quad 1 \leq j \leq N_S. \quad (4.14)$$

These functions are extended by zero to the rest of the boundary, i.e. $P_0^j(x) = P_1^j(x) = 0$ for $x \notin I_j$. In this basis, the boundary condition of Eq. (4.11) will take the form

$$\xi_k - i\zeta_k = U_{kl}(\xi_l + i\zeta_l), \quad k, l = 1, \dots, 2N_S, \quad (4.15)$$

where ξ_k and ζ_k are the coefficients of the Legendre expansion and are related to the linear functions of Eqs. (4.13) by

$$\xi_j = \langle P_0^j, L^j \rangle_{I_j} = \int_{x_j}^{x_j+h} P_0^j(x) L^j(x) dx = \frac{\sqrt{h}}{2}(a_{j+1} + a_j), \quad 1 \leq j \leq N_S, \quad (4.16a)$$

$$\xi_{j+N_S} = \langle P_1^j, L^j \rangle_{I_j} = \int_{x_j}^{x_j+h} P_1^j(x) L^j(x) dx = \frac{\sqrt{h}}{2\sqrt{3}}(a_{j+1} - a_j), \quad 1 \leq j \leq N_S, \quad (4.16b)$$

$$\zeta_j = \langle P_0^j, \dot{L}^j \rangle_{I_j} = \int_{x_j}^{x_j+h} P_0^j(x) \dot{L}^j(x) dx = \frac{\sqrt{h}}{2}(n_{j+1} + n_j), \quad 1 \leq j \leq N_S, \quad (4.16c)$$

$$\zeta_{j+N_S} = \langle P_1^j, \dot{L}^j \rangle_{I_j} = \int_{x_j}^{x_j+h} P_1^j(x) \dot{L}^j(x) dx = \frac{\sqrt{h}}{2\sqrt{3}}(n_{j+1} - n_j), \quad 1 \leq j \leq N_S. \quad (4.16d)$$

Moreover, the unitary matrix U_{kl} is defined by

$$U_{kl} = \begin{cases} \langle P_0^k, U^N P_0^l \rangle, & 1 \leq k, l \leq N_S, \\ \langle P_1^{k-N_S}, U^N P_0^l \rangle, & N_S + 1 \leq k \leq 2N_S, \quad 1 \leq l \leq N_S, \\ \langle P_0^k, U^N P_1^{l-N_S} \rangle, & 1 \leq k \leq N_S, \quad N_S + 1 \leq l \leq 2N_S, \\ \langle P_1^{k-N_S}, U^N P_1^{l-N_S} \rangle, & N_S + 1 \leq k, l \leq 2N_S. \end{cases} \quad (4.17)$$

As stated before, we need a finite element model where the restrictions to the boundary are linear functions and whose restrictions to the boundary of their normal derivatives are linear too. Moreover, the restriction of the functions at the border with the bulk region (see Fig. 4.1) have also to be linear. This latter condition guarantees a continuous matching with the base-functions at the bulk. To achieve this, we have chosen the following model in a square with eight nodes.

The reference square \mathcal{R}_S is depicted in Fig. 4.3. We will have on each square the following base-function:

$$\phi_i|_S = p_{1i}y^3x + p_{2i}y^3 + p_{3i}y^2x + p_{4i}y^2 + p_{5i}yx + p_{6i}y + p_{7i}x + p_{8i}, \quad (4.18)$$

where x is the coordinate parallel to the boundary and y is the coordinate normal to it. The coordinates with $y = 0$ will correspond to the boundary of the region while $y = 1$ represents the region of the square that touches the bulk. Notice that the polynomial is at most linear in x and that the derivative with respect to y is also linear in x . We shall consider that the pairs of interior nodes (denoted by \square) are problem nodes and that the pairs of exterior nodes (denoted by \diamond), called *boundary nodes*, are going to be determined by the boundary conditions and the values at the problem nodes. Notice that the choice of a polynomial of up to second order in the variable y would have given an unequal number of problem nodes and boundary nodes.

With this model, the value of the normal derivative at the node x_j , in a square of side h , is given by the expression:

$$n_j = \frac{1}{h} \left(-\frac{11}{2}a_j + 9b_j - \frac{9}{2}c_j + d_j \right). \quad (4.19)$$

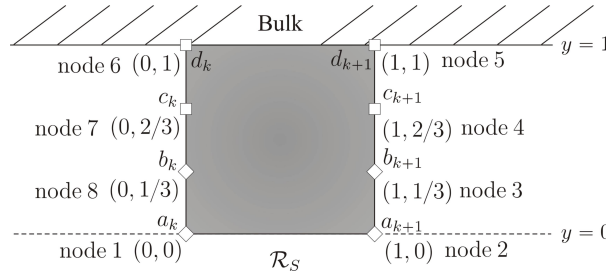


Fig. 4.3: Reference square \mathcal{R}_S . Parameters a, b, c, d are the value of the base-function at those nodes. Parameters a_k and a_{k+1} represent the values of the base-function at the boundary, and parameters d_k and d_{k+1} are the values at the region touching the bulk. The \square denote the problem nodes and the \diamond denote the boundary nodes.

Now we will use the boundary conditions, Eq. (4.15), to determine the value at the boundary nodes in terms of the problem nodes. Hence, we will substitute back Eq. (4.19) in Eqs. (4.16) and Eq. (4.15). Denoting by s a column vector with the values of a_j and b_j , and by w a column vector with the values of c_i and d_i

$$s^\top = [a_1, \dots, a_{N_S}, b_1, \dots, b_{N_S}], \quad w^\top = [c_1, \dots, c_{N_S}, d_1, \dots, d_{N_S}], \quad (4.20)$$

and having into account that at the boundary we have identified node x_0 with node x_{N_S} , we get the following equations in matrix form:

$$\begin{bmatrix} \mathcal{F}_0 \\ \mathcal{F}_1 \end{bmatrix} s = \begin{bmatrix} \mathcal{C}_0 \\ \mathcal{C}_1 \end{bmatrix} w, \quad (4.21a)$$

with

$$\begin{aligned} \mathcal{F}_0 = & \left(\frac{\sqrt{h}}{2} + i \frac{11}{4\sqrt{h}} \right) (\mathcal{N} + \mathcal{I}) \mathcal{L} - i \frac{9}{2\sqrt{h}} (\mathcal{N} + \mathcal{I}) \mathcal{R} \\ & - U_{[00]} \left[\left(\frac{\sqrt{h}}{2} - i \frac{11}{4\sqrt{h}} \right) (\mathcal{N} + \mathcal{I}) \mathcal{L} - i \frac{9}{2\sqrt{h}} (\mathcal{N} + \mathcal{I}) \mathcal{R} \right] \\ & - U_{[01]} \left[\left(\frac{\sqrt{h}}{2\sqrt{3}} - i \frac{11}{4\sqrt{3}\sqrt{h}} \right) (\mathcal{N} - \mathcal{I}) \mathcal{L} + i \frac{9}{2\sqrt{3}\sqrt{h}} (\mathcal{N} - \mathcal{I}) \mathcal{R} \right], \end{aligned} \quad (4.21b)$$

$$\begin{aligned} \mathcal{F}_1 = & \left(\frac{\sqrt{h}}{2\sqrt{3}} + i \frac{11}{4\sqrt{3}\sqrt{h}} \right) (\mathcal{N} - \mathcal{I}) \mathcal{L} - i \frac{9}{2\sqrt{3}\sqrt{h}} (\mathcal{N} - \mathcal{I}) \mathcal{R} \\ & - U_{[10]} \left[\left(\frac{\sqrt{h}}{2} - i \frac{11}{4\sqrt{h}} \right) (\mathcal{N} + \mathcal{I}) \mathcal{L} - i \frac{9}{2\sqrt{h}} (\mathcal{N} + \mathcal{I}) \mathcal{R} \right] \\ & - U_{[11]} \left[\left(\frac{\sqrt{h}}{2\sqrt{3}} - i \frac{11}{4\sqrt{3}\sqrt{h}} \right) (\mathcal{N} - \mathcal{I}) \mathcal{L} + i \frac{9}{2\sqrt{3}\sqrt{h}} (\mathcal{N} - \mathcal{I}) \mathcal{R} \right], \end{aligned} \quad (4.21c)$$

$$\begin{aligned} \mathcal{C}_0 = & -i \frac{9}{4\sqrt{h}} (\mathcal{N} + \mathcal{I}) \mathcal{L} + i \frac{1}{2\sqrt{h}} (\mathcal{N} + \mathcal{I}) \mathcal{R} \\ & + U_{[00]} \left[-i \frac{9}{4\sqrt{h}} (\mathcal{N} + \mathcal{I}) \mathcal{L} + i \frac{1}{2\sqrt{h}} (\mathcal{N} + \mathcal{I}) \mathcal{R} \right] \\ & + U_{[01]} \left[-i \frac{9}{4\sqrt{3}\sqrt{h}} (\mathcal{N} - \mathcal{I}) \mathcal{L} + i \frac{1}{2\sqrt{3}\sqrt{h}} (\mathcal{N} - \mathcal{I}) \mathcal{R} \right], \end{aligned} \quad (4.21d)$$

$$\begin{aligned} \mathcal{C}_1 = & -i \frac{9}{4\sqrt{3}\sqrt{h}} (\mathcal{N} - \mathcal{I}) \mathcal{L} + i \frac{1}{2\sqrt{3}\sqrt{h}} (\mathcal{N} - \mathcal{I}) \mathcal{R} \\ & + U_{[10]} \left[-i \frac{9}{4\sqrt{h}} (\mathcal{N} + \mathcal{I}) \mathcal{L} + i \frac{1}{2\sqrt{h}} (\mathcal{N} + \mathcal{I}) \mathcal{R} \right] \\ & + U_{[11]} \left[-i \frac{9}{4\sqrt{3}\sqrt{h}} (\mathcal{N} - \mathcal{I}) \mathcal{L} + i \frac{1}{2\sqrt{3}\sqrt{h}} (\mathcal{N} - \mathcal{I}) \mathcal{R} \right], \end{aligned} \quad (4.21e)$$

where

$$U = \begin{pmatrix} U_{[00]} & U_{[01]} \\ U_{[10]} & U_{[11]} \end{pmatrix} \quad (4.22)$$

is the block-wise decomposition of U , with blocks of size $N_S \times N_S$ that corresponds to the block-wise structure of Eq. (4.17). The matrix \mathcal{I} is the $N_S \times N_S$ identity matrix, \mathcal{N} is the $N_S \times N_S$ row cyclic-shift matrix defined as follows:

$$N = \begin{pmatrix} 0 & 1 & 0 & \cdots & 0 \\ \vdots & \ddots & \ddots & & \vdots \\ \vdots & & \ddots & \ddots & 0 \\ 0 & & & \ddots & 1 \\ 1 & 0 & \cdots & \cdots & 0 \end{pmatrix}.$$

The matrix \mathcal{L} is the $N_S \times 2N_S$ matrix whose first N_S columns are the identity $N_S \times N_S$ matrix and the rest is zero $\mathcal{L} = [\mathcal{I}, \mathbf{0}]$. Similarly, $\mathcal{R} = [\mathbf{0}, \mathcal{I}]$ is the $N_S \times 2N_S$ matrix whose last N_S columns are the identity matrix.

Given a vector w , i.e. the vector with the values of the nodes c_j and d_j of Eq. (4.20), the linear system defined in Eqs. (4.21) determines a linear system of equations with unknown s , i.e. the vector with the values of the nodes a_j and b_j . Therefore, we need to choose a set of vectors $\{w^k\}_{1 \leq k \leq 2N_S}$ furnishing a set of linearly independent functions. The most natural choice for this

set is the canonical basis of \mathbb{R}^{2N_S} . This choice leads to the set of linear systems

$$\mathcal{F}s = \mathcal{C}, \quad (4.23)$$

with $\mathcal{F}, \mathcal{C} \in \mathbb{C}^{2N_S \times 2N_S}$ the coefficient and independent matrices of the linear system in Eq. (4.21a). We use the same symbol s to denote the solutions of this family of linear systems. This family depends on the unitary operator U and is overdetermined. In order to solve it, we will use the singular value decomposition (SVD for short) of the coefficient matrix \mathcal{F} , cf. [13].

The fact that the matrix \mathcal{F} is not of full rank tells us that there is a freedom in the choice of $2N_S - \text{rank}(\mathcal{F})$ parameters. For every choice of these parameters, one gets an alternative set of solutions of the linear system (4.23). Instead of setting all these parameters to zero, we will additionally solve a least squares problem to fix these parameters in such a way that the solution is the one that deviates the less from the Neumann case. The Neumann case is taken as a reference set of boundary functions with value $a_j = 1$ at one node of the boundary and $a_k = 0$, $k \neq j$ at the remaining nodes of the boundary. The coefficients $\{b_j\}$ are chosen such that the normal derivatives, given by Eq. (4.19), vanish. For the choices of the coefficients $\{c_j\}$ and $\{d_j\}$ as the canonical basis of \mathbb{R}^{2N_S} , the reference matrix X_{Neumann} is as follows

$$X_{\text{Neumann}} = [X_c \ X_d], \quad X_c \begin{bmatrix} \mathcal{I} \\ \frac{10}{4}\mathcal{I} \end{bmatrix}, \quad X_d \begin{bmatrix} \mathcal{I} \\ \frac{1}{2}\mathcal{I} \end{bmatrix}. \quad (4.24)$$

The reason for looking for the least squares approximation that better fits X_{Neumann} is two-fold:

First, it minimises the number of boundary elements where the boundary functions are different from zero. The performance of the algorithm is greatly increased in this way since it reduces polynomially the number of operations needed to compute the matrices of Eq. (4.4). Recall that, in general, the boundary functions are non-local and spread along the boundary. Thus, the computations of the matrices M , F and B involve sums over all the squares of the boundary. Although, in principle, there are situations with non-local boundary conditions that necessarily spread along the full boundary, in practice the most usual situations require non-vanishing of the boundary functions in a very limited number of boundary elements. For instance, periodic and quasi-periodic boundary conditions can be implemented with boundary functions that are non-vanishing only at a pair of opposed sites of the grid.

Second, the least squares problem solution tries to get the non-vanishing boundary values as close to the value 1 as possible, which improves the behaviour of the implementation of natural boundary conditions. In addition to this, the computation of the least squares problem solution can be achieved without almost no additional computational cost since the factorisation provided by the singular value decomposition can be used directly to compute the least squares solution.

Let $\mathcal{F} = \mathcal{W}\mathcal{S}\mathcal{V}^\dagger$ be the SVD of the matrix \mathcal{F} . The relation between the complete and reduced SVD factorisations is given in block-wise matrix notation as:

$$\mathcal{W} =: [\mathcal{W}_{\text{red}}, \mathcal{W}_{\text{null}}], \quad \mathcal{S} =: \begin{bmatrix} \mathcal{S}_{\text{red}} & 0 \\ 0 & 0 \end{bmatrix}, \quad \mathcal{V} =: [\mathcal{V}_{\text{red}}, \mathcal{V}_{\text{null}}]. \quad (4.25)$$

Before solving the system one has to check that the linear system is compatible within numerical error, i.e.

$$(\mathbb{I} - \mathcal{W}_{\text{red}}\mathcal{W}_{\text{red}}^\dagger)\mathcal{C} = 0.$$

Deviations from this serve as a measure of the goodness of the solution. The inhomogeneous solution of the linear system (4.23) is given by $s_{ih} = \mathcal{V}_{\text{red}}x$, where x is the solution of the reduced linear system

$$\mathcal{S}_{\text{red}}x = \mathcal{W}_{\text{red}}^\dagger\mathcal{C}. \quad (4.26)$$

The general solution of the linear system is therefore given by

$$s = \mathcal{V}_{\text{red}}x + \mathcal{V}_{\text{null}}\varepsilon, \quad (4.27)$$

where $\varepsilon \in \mathbb{C}^{2N_S - \text{rank}(\mathcal{F})}$ is the family of parameters that we will fix by means of the least squares solution. Among all the possible solutions, we want the one that minimises

$$\|s - X_{\text{Neumann}}\|^2,$$

where the norm is the euclidean norm in \mathbb{R}^{2N_S} . The least squares solution is

$$\varepsilon = \mathcal{V}_{\text{null}}^\dagger (X_{\text{Neumann}} - \mathcal{V}_{\text{red}}x) = \mathcal{V}_{\text{null}}^\dagger X_{\text{Neumann}}. \quad (4.28)$$

Substituting back in Eq. (4.27) we get finally

$$s = \mathcal{V}_{\text{red}}x + \mathcal{V}_{\text{null}}\mathcal{V}_{\text{null}}^\dagger X_{\text{Neumann}}. \quad (4.29)$$

Notice that there was no need to compute further factorisations of the matrices, and hence, the additional computational cost is just the multiplication of the matrices at the right hand side of Eq. (4.29).

Let $r := \text{rank}(\mathcal{F}) \leq 2N_S$ be the rank of the matrix \mathcal{F} . This means that the set of linear systems of Eq. (4.23) provides r linearly independent base-functions at the boundary satisfying the boundary conditions. In addition to the solutions above, we need to consider an additional set of linearly independent boundary functions satisfying trivially the boundary conditions, i.e. $a_j = 0$, $n_j = 0$ for $1 \leq j \leq N_S$. This is necessary to provide a complete basis for the FEM. Having into account Eq. (4.19), this implies that we can consider another family of boundary functions determined by

$$a_j = 0, \quad b_j = \frac{1}{2}c_j - \frac{1}{9}d_j, \quad 1 \leq j \leq n. \quad (4.30)$$

This family is clearly linearly independent from the family obtained as solution of (4.23). Hence, we have two different families of base-functions at the boundary. The base-functions satisfying Eq. (4.30), that will be called *1st family* from now on, and the solutions of Eq. (4.23), that will be called *2nd family*.

Once the finite element model is determined, we have to compute the entries of the matrices M , B and F corresponding to the base-functions at the boundary, cf. Eq. (4.4). Those are, according to Eq. (4.18), as follows:

$$\phi_i = \begin{cases} p_{1i}^1 y^3 x + p_{2i}^1 y^3 + p_{3i}^1 y^2 x + p_{4i}^1 y^2 + p_{5i}^1 y x + p_{6i}^1 y + p_{7i}^1 x + p_{8i}^1, & \text{square 1} \\ p_{1i}^2 y^3 x + p_{2i}^2 y^3 + p_{3i}^2 y^2 x + p_{4i}^2 y^2 + p_{5i}^2 y x + p_{6i}^2 y + p_{7i}^2 x + p_{8i}^2, & \text{square 2} \\ \vdots & \vdots \\ p_{1i}^{N_S} y^3 x + p_{2i}^{N_S} y^3 + p_{3i}^{N_S} y^2 x + p_{4i}^{N_S} y^2 + p_{5i}^{N_S} y x + p_{6i}^{N_S} y + p_{7i}^{N_S} x + p_{8i}^{N_S}, & \text{square } N_S \end{cases} \quad (4.31)$$

where the x, y coordinates correspond to the parallel and normal direction on each square with respect to the boundary. Notice that the base-functions are cubic in y and linear in x , with $i = 1, \dots, N_S + r$, where N_S is the number of squares at the boundary and r is the rank of \mathcal{F} .

The linear transformation that maps the reference square in Fig. 4.3 to any square is

$$\begin{pmatrix} x \\ y \end{pmatrix} = \begin{pmatrix} x_1 \\ y_1 \end{pmatrix} + \begin{pmatrix} x_2 - x_1 & 0 \\ 0 & y_6 - y_1 \end{pmatrix} \begin{pmatrix} \eta \\ \xi \end{pmatrix}, \quad (4.32)$$

and the first derivatives of the coordinates in the reference square with respect to x and y are

$$\begin{pmatrix} \eta_x & \eta_y \\ \xi_x & \xi_y \end{pmatrix} = \begin{pmatrix} \frac{1}{x_2 - x_1} & 0 \\ 0 & \frac{1}{y_6 - y_1} \end{pmatrix}. \quad (4.33)$$

Finally, to compute the integrals (4.3a) and (4.3b), one needs to compute the contributions of each square to the matrix elements, i.e. $M_{ij}|_{S_k}$, $B_{ij}|_{S_k}$ and $F_{ij}|_{S_k}$. Each one of these contributions is the result of the integral of a certain polynomial on the reference square \mathcal{R}_S in terms of the values of the nodes. It is important to remark that the contribution to $F_{ij}|_{S_k}$ has to be done by integrating in the counterclockwise orientation of the boundary.

4.3. Convergence of the finite element model. In the previous subsection, we have introduced a finite element model to approximate the spectral problem of Eq. (3.1). It remains to show that the finite element model is indeed an approximating family, cf. Def. 3.1. First of all, let us remark that the condition showed in Eq. (3.5) is satisfied as a consequence of choosing piecewise continuous functions as finite element model. In order that our family becomes an approximating family, we just need to choose U^N as the unique unitary operator which corresponds to a projector P_{U^N} , and a self-adjoint operator A_{U^N} satisfying Assumption 1. The following result shows a particular simple choice that gathers these conditions.

PROPOSITION 4.1. *Let P_U and A_U be the operators defining the spectral problem of Eq. (3.1). Suppose that P_U is a continuous operator with respect to the Sobolev norm $\mathcal{H}^{1/2}(\partial\Omega)$. Let K^N be the orthogonal projectors onto the subspaces defined by the piecewise linear continuous functions parameterised by the Legendre polynomials of Eq. (4.14) and such that*

$$\|K^N \varphi\|_{\mathcal{H}^{1/2}(\partial\Omega)} \leq c \|\varphi\|_{\mathcal{H}^{1/2}(\partial\Omega)} .$$

Let

$$P_{U^N} := K^N P_U K^N \quad \text{and} \quad A_{U^N} := K^N A_U K^N ,$$

then, P_{U^N} and A_{U^N} satisfy Assumption 1.

Proof. Let us check first point i):

$$\begin{aligned} \|(K^N P_U K^N - P_U)\varphi\|_{\mathcal{H}^{1/2}(\partial\Omega)} &\leq \|(K^N - \mathbb{I})P_U\varphi\|_{\mathcal{H}^{1/2}(\partial\Omega)} + \|(K^N P_U(\mathbb{I} - K^N)\varphi\|_{\mathcal{H}^{1/2}(\partial\Omega)} \\ &\leq \|(K^N - \mathbb{I})P_U\varphi\|_{\mathcal{H}^{1/2}(\partial\Omega)} + c\|(\mathbb{I} - K^N)\varphi\|_{\mathcal{H}^{1/2}(\partial\Omega)} , \end{aligned}$$

where we have used that P_U is continuous with respect to the Sobolev norm $\mathcal{H}^{1/2}(\partial\Omega)$. Since K^N is the projector onto the space of continuous piecewise linear functions at the boundary and

$$\|(\mathbb{I} - K^N)\varphi\|_{\mathcal{H}^{1/2}(\partial\Omega)} \leq \|(\mathbb{I} - K^N)\varphi\|_{\mathcal{H}^1(\partial\Omega)} ,$$

the right hand side can be chosen smaller than any ϵ by choosing the lattice spacing small enough.

Let us now prove ii). Let $\psi, \varphi \in \mathcal{L}^2(\partial\Omega)$, then,

$$\begin{aligned} \langle \psi, (A_{U^N} - A_U)\varphi \rangle &= \langle \psi - K^N \psi, (A_{U^N} - A_U)\varphi \rangle + \langle K^N \psi, (A_{U^N} - A_U)(\varphi - K^N \varphi) \rangle \\ &\quad + \langle K^N \psi, (A_{U^N} - A_U)K^N \varphi \rangle \\ &\leq 2\|(\mathbb{I} - K^N)\psi\|_{A_U} \|\varphi\| + 2\|K^N \psi\|_{A_U} \|(\mathbb{I} - K^N)\varphi\| \\ &\quad + \langle \psi, (A_{U^N} - K^N A_U K^N)\varphi \rangle . \end{aligned}$$

The third factor at the right hand side of the inequality is trivially zero, and the other two go to zero by the same argument of the previous point. \square

5. The pseudocode. In this section we show how to construct the algorithm described in the previous section in a schematic way. We present it in 5 steps.

1) Inputs and outputs:

Inputs:

- n , that is the number of nodes in which are discretised both axis (remember that for simplicity, we have considered $n = m$). To obtain the triangularisation in Fig. 4.1, n must be odd.
- U_{kl} , that is the unitary matrix that contains the information of the boundary conditions. The matrix U_{kl} defines the approximate boundary conditions implicitly through Eq. (4.15) and is the approximation of the unitary operator U defining the problem, cf. Section 2.

With this ordering, odd nodes are star-like nodes and even nodes are diamond-like nodes, see Figs. 4.2. Notice also that because of the symmetry of the triangularisation, the number of the different elements that appear at the bulk part of matrices M and B reduce to a very small number, concretely 4:

- If $i = j$ odd, we have a star-like configuration (\star) where both base-functions ϕ_i and ϕ_j have value 1 in the center and 0 in the rest.
- If $i = j$ even, we have the same as before but for a diamond-like configuration (\diamond).
- If $i \neq j$ both odd, we have that there is only non vanishing contribution in the two triangles that share the edge that links i with j .
- If $i \neq j$ one odd and other even, again, we have that there is only non vanishing contribution in the two triangles with edge (i, j) , but in this case, these two triangles belong to different squares.

Therefore, we only need to compute the value of the matrix elements of M and B once for each case, using formulas (4.9a) and (4.9b) respectively, to know the value of the matrix elements of M and B for all elements corresponding to the bulk:

$$M_{ij}, B_{ij} = \begin{cases} M_{11}, B_{11}, & \text{if } i = j \text{ and odd,} \\ M_{22}, B_{22}, & \text{if } i = j \text{ and even,} \\ M_{(N_S-7)1}, B_{(N_S-7)1}, & \text{if } i \neq j, \text{ both odd and close neighbours,} \\ M_{(N_S-7)2}, B_{(N_S-7)2}, & \text{if } i \neq j \text{ with one odd and other even and close neighbours,} \\ 0, & \text{otherwise,} \end{cases} \quad (5.3)$$

where $i, j = 1, \dots, (n-2)^2$.

3) Base-functions at the boundary: In the model, we have two different families of base-functions at the boundary. The first one is a family of $2N_S$ linearly independent base-functions that satisfy the boundary conditions trivially. We have called this family of base-functions *1st family*. The second one is a family of r linearly independent functions that satisfy the boundary conditions in Eq. (4.11). We have called this family of base-functions *2nd family*.

Remember that, as stated in Section 4.2, there is complete freedom in the choice of the parameters c_k^i and d_k^i (nodes depicted by \square in Fig. 4.1), $i = 1, \dots, 2N_S$, $k = 1, \dots, N_S$. Hence, for simplicity, we have divided the *1st family* in two subfamilies of N_S base-functions. One with $c_k^i = \delta_{ki}$ and $d_k^i = 0$ and other with $c_k^i = 0$ and $d_k^i = \delta_k^i$, where now $i = 1, \dots, N_S$ is the label of the base-function and $k = 1, \dots, N_S$ is the label that indicates which edge of that base-function we are considering, (see Fig. 5.1). After substituting this particular choice in (4.30), we get the parameters b_k^i :

$$d_k^i = 0, \quad c_k^i = \delta_{ki}, \quad b_k^i = \frac{1}{2}\delta_{ki}, \quad a_k^i = 0, \quad 1^{st} \text{ family}[c], \quad (5.4a)$$

$$d_k^i = \delta_{ki}, \quad c_k^i = 0, \quad b_k^i = -\frac{1}{9}\delta_{ki}, \quad a_k^i = 0, \quad 1^{st} \text{ family}[d]. \quad (5.4b)$$

Let us remark that because of the definition of the *1st family* in Eqs. (5.4), the squares in which these base-functions have non-vanishing contribution are the two squares that share the edge with $k = i$. Knowing *a priori* which squares have vanishing contribution is crucial in saving time for the computation of the matrix elements in M , B and F .

We explain now the routine to compute the values at the nodes of the base-functions corresponding to the *2nd family*:

- Implementation of the linear system of Eqs. (4.21), Eq. (4.23).
- The independent coefficients \mathcal{C} are defined for the values $c_k^i = \delta_k^i$ and $d_k^i = 0$, which correspond to what is called the *2nd family*[c] and the values $c_k^i = 0$ and $d_k^i = \delta_k^i$, which correspond to the *2nd family*[d].
- Computation of the SVD of the matrix $\mathcal{F} = \mathcal{W}\mathcal{S}\mathcal{V}^\dagger$.

- Determination of r (the rank of \mathcal{F}) by counting the non-zero diagonal elements of \mathcal{S} (bigger than numerical error).
- Check the compatibility of the linear system: $(\mathbb{I} - \mathcal{W}_{\text{red}} \mathcal{W}_{\text{red}}^\dagger) \mathcal{C} = 0$ within numerical error.
- Computation of the inhomogeneous solution: $x = \mathcal{S}_{\text{red}}^{-1} \mathcal{U}_{\text{red}}^\dagger \mathcal{C}$.
- Computation of the least squares solution that better approximates the Neumann problem.

$$s = \mathcal{V}_{\text{red}} x + \mathcal{V}_{\text{null}} \mathcal{V}_{\text{null}}^\dagger X_{\text{Neumann}} .$$

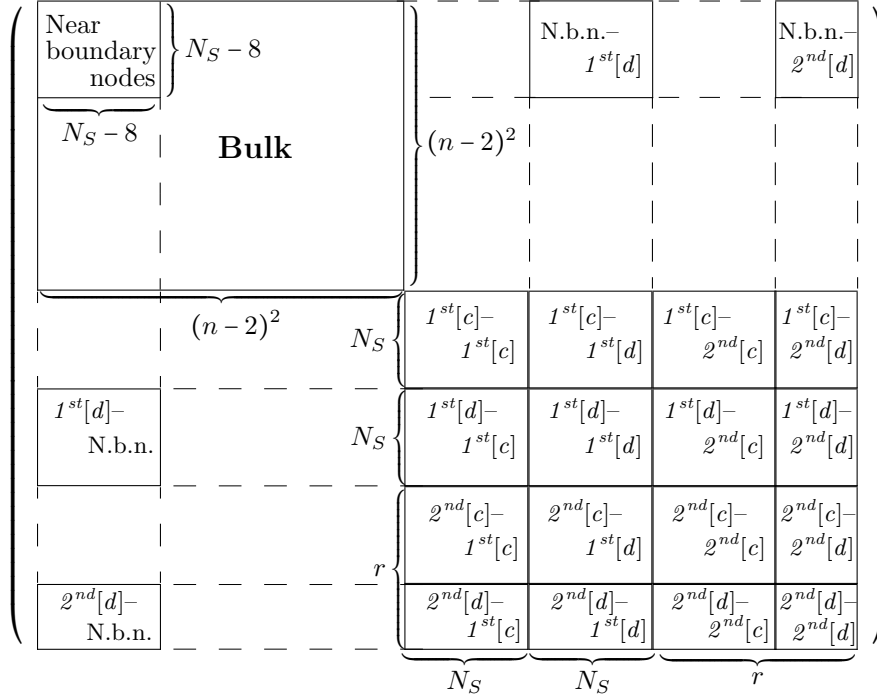


Fig. 5.2: Blockwise structure of the matrices M , B and F . The matrix F has non-vanishing contribution only at the bottom right block of size $r \times r$. Those are the matrix elements involving inner products of base-functions of the 2^{nd} family.

4) Matrix elements at the boundary: At Step 2) we have computed the matrix elements of matrices M and B at the bulk. Now we compute the remaining matrix elements and the matrix F . Notice that the matrices M and B are manifestly Hermitean, but this is not the case for the matrix F . However, even if Eq. (4.3b) is not Hermitean in general, the boundary conditions imposed on the base-functions at the boundary guarantee that this is so (up to numerical error). Hence, we just need to compute the elements of M_{ij} , B_{ij} and F_{ij} for $i \geq j$.

At Step 2) we have sorted the first row of the bulk in counterclockwise order, see Fig. 5.1. We did so because the base-functions at the bulk corresponding to such nodes are the only ones that will have non vanishing contribution with the $[d]$ parts of the two families of base-functions at the boundary.

If we order the base-functions at the boundary after the base-functions at the bulk and we put them in this order: 1^{st} family $[c]$, 1^{st} family $[d]$, 2^{nd} family $[c]$, 2^{nd} family $[d]$, the matrices M , B and F will have the structure showed in Fig. 5.2. The elements outside the blocks, in both matrices, are 0. Notice that we need to take only r linearly independent base-functions of the 2^{nd} family. Notice also that for the construction of these structures, we have supposed that $r > N_S$. In the case in which $r \leq N_S$, we have to remove the blocks involving the base-functions of 2^{nd} family $[d]$ and the rows and columns of the blocks involving the 2^{nd} family $[c]$ have then size r instead of N_S .

The elements of the blocks are computed by means of the formulas in Eq. (4.31). The number of computations that depend on the choice of different boundary conditions is limited to the elements of the 2^{nd} family. The base-functions of the 1^{st} family have all the same shape shifted along the boundary. Hence, they give contribution to matrix elements only if their support share at least one edge. Notice that the matrix elements corresponding to the pairings between base-functions of the subfamilies $[d]$ have non-vanishing contribution at the bulk. Hence, one has to add to these elements the corresponding contribution on the triangles of the bulk. Because of this contribution, it is necessary to distinguish between even and odd nodes (star-like and diamond-like, see Fig. 4.2) and the nodes at the corners of Ω .

Below, is shown an example of the computation of the block of the matrix M corresponding to the pairing 2^{nd} family $[d]$ – 1^{st} family $[d]$:

- 2^{nd} family $[d]$ – 1^{st} family $[d]$: The indexes of the elements of this block are $i = (n-2)^2 + 3N_S + l$ and $j = (n-2)^2 + N_S + l'$ with $l = 1, \dots, r - N_S$ and $l' = 1, \dots, N_S$. Because both are a $[d]$ part of a family, we have to add the contribution at the bulk. Notice that this block must be added only in the case in which $r > N_S$, otherwise we do not have base-functions of 2^{nd} family $[d]$:

$$M_{ij} = \begin{cases} \sum_{k=l'-1}^{l'} M_{((n-2)^2+3N_S+l) ((n-2)^2+N_S+l')} \Big|_{S_k} + \frac{M_{11}}{4}, & \text{if } l = l' = \{1, n, 2n-1, \\ & 3n-2\} \text{ and } S_{l'-1} \text{ or } S_{l'} \\ & \text{are in } \mathcal{S}_{2[d]}(l), \\ \sum_{k=l'-1}^{l'} M_{((n-2)^2+3N_S+l) ((n-2)^2+N_S+l')} \Big|_{S_k} + \frac{M_{22}}{2}, & \text{if } l = l' \text{ even and } S_{l'-1} \text{ or} \\ & S_{l'} \text{ are in } \mathcal{S}_{2[d]}(l), \\ \sum_{k=l'-1}^{l'} M_{((n-2)^2+3N_S+l) ((n-2)^2+N_S+l')} \Big|_{S_k} + \frac{M_{11}}{2}, & \text{if } l = l' \text{ odd and } S_{l'-1} \text{ or} \\ & S_{l'} \text{ are in } \mathcal{S}_{2[d]}(l), \\ \sum_{k=l'-1}^{l'} M_{((n-2)^2+3N_S+l) ((n-2)^2+N_S+l')} \Big|_{S_k} + \frac{M_{(N_S-7)1}}{2}, & \text{if } l = l' + 1 \text{ and } S_{l'-1} \text{ or} \\ & S_{l'} \text{ are in } \mathcal{S}_{2[d]}(l), \\ \sum_{k=l'-1}^{l'} M_{((n-2)^2+3N_S+l) ((n-2)^2+N_S+l')} \Big|_{S_k}, & \text{if } l \neq l' + 1 \text{ and } S_{l'-1} \text{ or} \\ & S_{l'} \text{ are in } \mathcal{S}_{2[d]}(l), \\ 0, & \text{otherwise,} \end{cases}$$

where $\mathcal{S}_{2[d]}(l)$ denotes the squares at the support of the base-function l of 2^{nd} family $[d]$, and $S_{l'}$ denotes the square l' .

5) **Coefficients:** Solve the generalised eigenvalue problem, Eq. (4.4), to obtain the coefficients of the expansion of the eigenvectors and the eigenvalues.

6. Numerical examples. In this section we compute explicitly the solutions of several situations to show the capabilities of the algorithm. This will serve not only for checking the effectiveness of the procedure but also to show how to chose the input matrix U in order to obtain different boundary conditions. In all the examples the parameter that fixes the discretisation size is taken to be the number n of divisions of one side of the boundary.

6.1. Dirichlet and Neumann boundary conditions. As explained in Section 4.2, the unitary matrix that serves as input is an approximation to the space of piecewise linear functions with basis the Legendre polynomials at each site of the discretisation of the boundary. The unitary matrix has the block-wise linear structure

$$U = \begin{bmatrix} U_{[00]} & U_{[01]} \\ U_{[10]} & U_{[11]} \end{bmatrix}, \quad (6.1)$$

where $U_{[00]}, \dots, U_{[11]}$ are the blocks corresponding to Eq. (4.17). If N_S is the number of finite elements at the boundary, the blocks $U_{[ij]}$ are $N_S \times N_S$ and therefore U is of shape $2N_S \times 2N_S$.

As can be read from Eq. (2.3), Dirichlet and Neumann boundary conditions are almost trivial to implement. The former corresponds to the choice $U = -\mathbb{I}$ and the latter for $U = \mathbb{I}$. From Eq. (2.3) or its approximated counterpart, Eq. (4.11) and Eq. (4.15), it is clear that the former imposes $\varphi = 0$ while the latter imposes $\dot{\varphi} = 0$.

In this simple situation, the linear system (4.23) returns the base-functions at the boundary of these well-studied problems and, in both cases, the solutions obtained agree in accuracy with the expected behaviour of a FEM with piecewise linear polynomials. Results are shown in Table 6.1

| | Eigenvalue | | | | | | | |
|-----------|------------|---------|---------|---------|---------|---------|----------|----------|
| | 1 | 2 | 3 | 4 | 5 | 6 | 7 | 8 |
| Dirichlet | 19.7402 | 49.3536 | 49.3536 | 78.9733 | 98.7159 | 98.7159 | 128.3461 | 128.3461 |
| Exact | 19.7392 | 49.3480 | 49.3480 | 78.9568 | 98.6960 | 98.6960 | 128.3048 | 128.3048 |
| Neumann | -0.0000 | 9.8717 | 9.8717 | 19.7480 | 39.4810 | 39.4965 | 49.3730 | 49.3731 |
| Exact | 0 | 9.8696 | 9.8696 | 19.7392 | 39.4784 | 39.4784 | 49.3480 | 49.3480 |

Table 6.1: Dirichlet and Neumann eigenvalues for $n = 201$ and the exact solutions respectively.

6.2. Robin boundary conditions. This is an example of a situation where natural boundary conditions are considered. These boundary conditions for the Laplace operator are written as

$$\dot{\varphi} = \Lambda \varphi .$$

Notice that the solutions will not be calculated in the standard way, that is, using Neumann boundary conditions, i.e. $U = \mathbb{I}$, and then calculating the matrix F , cf. Eq. (4.3b) and Eq. (4.4), associated to them by calculating the scalar products $\langle \varphi, \Lambda \varphi \rangle_{\partial\Omega}$. Instead, we will do it by considering the unitary matrix

$$U_{kl} = e^{i\alpha} \cdot \delta_{kl} \tag{6.2}$$

as input for the problem. Let us justify the choice of this unitary matrix. Consider the unitary operator on $\mathcal{L}^2(\partial\Omega)$ defined by:

$$U\varphi = e^{i\alpha}\varphi . \tag{6.3}$$

Simple algebraic manipulations on Eq. (2.3) show that this is equivalent to

$$\dot{\varphi} = -\tan\left(\frac{\alpha}{2}\right)\varphi, \quad \text{with } \alpha \neq \pm\pi . \tag{6.4}$$

The case $\alpha = \pm\pi$, corresponds to $U = -\mathbb{I}$, i.e. Dirichlet boundary conditions. The Robin parameter is therefore $\Lambda = -\tan\left(\frac{\alpha}{2}\right)$. Since this unitary operator is a constant multiplication operator, its representation in the Legendre basis expansion is again a constant multiplication operator, thus, we get (6.2).

Notice that the behaviour for positive and negative values of α is very different. While $\alpha > 0$ leads to positive definite self-adjoint extensions of the Laplace operator, for $\alpha < 0$ the problem is no longer positive defined and negative eigenvalues appear. Nevertheless, it is still lower semi-bounded, cf. [14, 16, 3], and thus the convergence is ensured. As already happens in the one-dimensional version of this procedure, cf. [18], convergence for the $\alpha < 0$ case is slower than for the $\alpha > 0$ situation. This is expected to happen because the eigenvalue problem for Robin boundary conditions with positive parameter presents locking, cf. [7], if the spectrum of the unitary operator is close to $\{-1\}$, i.e. $\alpha \rightarrow -\pi$. In Table 6.2 and Table 6.3, are shown the calculated eigenvalues for $\alpha = -0.9\pi$ and for $\alpha = 0.9\pi$, respectively, for different discretisation sizes.

| n | Eigenvalue | | | | | | | |
|-----|------------|----------|----------|----------|---------|---------|---------|---------|
| | 1 | 2 | 3 | 4 | 9 | 10 | 11 | 12 |
| 101 | -64.7361 | -63.4717 | -63.4717 | -62.1488 | 28.7944 | 31.6599 | 31.6599 | 36.1463 |
| 153 | -68.8114 | -67.7815 | -67.7815 | -66.7229 | 27.8643 | 29.6896 | 29.6896 | 32.9647 |
| 201 | -71.0235 | -70.1025 | -70.1025 | -69.1627 | 27.4320 | 28.7390 | 28.7390 | 31.4213 |
| 251 | -72.5633 | -71.7112 | -71.7112 | -70.8456 | 27.1572 | 28.1208 | 28.1208 | 30.4139 |

 Table 6.2: Robin eigenvalues for $\alpha = -0.9\pi$ for discretisation sizes $n = 101, 153, 201, 251$.

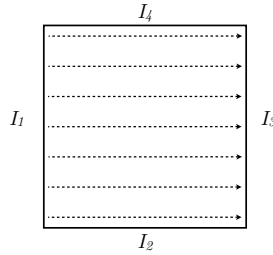
| n | Eigenvalue | | | | | | | |
|-----|------------|---------|---------|---------|---------|---------|---------|---------|
| | 1 | 2 | 3 | 4 | 5 | 6 | 7 | 8 |
| 101 | 11.7493 | 30.5681 | 30.5681 | 49.2777 | 64.7353 | 64.9841 | 83.4756 | 83.4756 |
| 153 | 11.7108 | 30.4944 | 30.4944 | 49.2079 | 64.6621 | 64.8201 | 83.3920 | 83.3920 |
| 201 | 11.6927 | 30.4598 | 30.4598 | 49.1745 | 64.6283 | 64.7460 | 83.3540 | 83.3540 |
| 251 | 11.6811 | 30.4377 | 30.4377 | 49.1528 | 64.6067 | 64.6996 | 83.3300 | 83.3300 |

 Table 6.3: Robin eigenvalues for $\alpha = -0.9\pi$ for discretisation sizes $n = 101, 153, 201, 251$.

6.3. Periodic boundary conditions. In this example we consider periodic boundary conditions. These constitute an example of purely essential boundary conditions. The convenience of choosing the Legendre basis expansion at each interval of the boundary will be manifest with this example. Let us introduce first the unitary operator that implements the exact boundary conditions on the square $[0, 1] \times [0, 1]$. We will impose periodic boundary conditions along opposed sites of the square. The unitary operator that corresponds to periodic boundary conditions has a block-wise structure according to the decomposition of the Hilbert space at the boundary corresponding to the four sides of the square depicted in Fig. 6.1, cf. [16, Example 5.2],

$$\mathcal{L}^2(\partial\Omega) = \mathcal{L}^2(I_1) \oplus \mathcal{L}^2(I_2) \oplus \mathcal{L}^2(I_3) \oplus \mathcal{L}^2(I_4). \quad (6.5)$$

Here, $\mathcal{L}^2(I_i) = \mathcal{L}^2(I_j)$, $i, j = 1, \dots, 4$.


 Fig. 6.1: Identification of the opposite sites of the square that gives rise to periodic boundary conditions. Only the identification between I_1 and I_3 is depicted.

Notice that a direct identification $I_1 = I_3$ and $I_2 = I_4$ would not let to periodic boundary conditions since both intervals have the same orientation. On the contrary, we want the left end of I_1 to be identified with the right end of I_3 , and equivalently for I_2 and I_4 . This implies that, in addition to this identification, we need to use an orientation reversing diffeomorphism. In coordinates relative to the centre of each interval, the latter takes the form $T : x \rightarrow -x$. Therefore, in the block-wise structure coming from the decomposition (6.5), the unitary operator takes the

form

$$U = \begin{bmatrix} 0 & 0 & T^* & 0 \\ 0 & T^* & 0 & 0 \\ T^* & 0 & 0 & 0 \\ 0 & 0 & 0 & T^* \end{bmatrix}, \quad (6.6)$$

where T^* denotes the pull-back under the diffeomorphism. This is the unitary operator implementing the exact boundary condition of the problem. Inserting this unitary operator in Eq. (2.3), and after some manipulations, it is easy to obtain that this is equivalent to

$$\gamma(\Phi)|_{I_1} = T^* \gamma(\Phi)|_{I_3}$$

and similarly for I_2 and I_4 .

Now, we need to express this unitary operator in the basis of the Legendre polynomials, see Eqs. (4.17). Assume first that we take the coarsest FE approximation of the boundary that is possible in this setting. That is, the discretisation given by the four intervals I_i , $i = 1, \dots, 4$. For this coarse approximation, the matrix U_{kl} is an 8×8 unitary matrix. Since the basis for the finite elements approximation at the boundary is given in terms of Legendre polynomials, most of the terms cancel out except:

$$\begin{aligned} \langle P_0^1, UP_0^3 \rangle &= \langle P_0^3, UP_0^1 \rangle = \langle P_0^2, UP_0^4 \rangle = \langle P_0^4, UP_0^2 \rangle = 1, \\ \langle P_1^1, UP_1^3 \rangle &= \langle P_1^3, UP_1^1 \rangle = \langle P_1^2, UP_1^4 \rangle = \langle P_1^4, UP_1^2 \rangle = -1. \end{aligned}$$

The difference in sign comes from the fact that the orientation reversing diffeomorphism leaves the even order Legendre polynomials invariant while the odd order polynomials change sign. Extending this result to the general situation, where each side of the square is divided into n intervals, is straightforward. The unitary matrix U_{kl} takes the form

$$U_{kl} = \begin{bmatrix} U_0 & 0 \\ 0 & -U_0 \end{bmatrix} \in \mathbb{C}^{8n \times 8n}, \quad U_0 = \begin{bmatrix} 0 & 0 & P & 0 \\ 0 & P & 0 & 0 \\ P & 0 & 0 & 0 \\ 0 & 0 & 0 & P \end{bmatrix} \in \mathbb{C}^{4n \times 4n}, \quad P = \begin{bmatrix} 0 & & 1 \\ & \ddots & \\ 1 & & 0 \end{bmatrix} \in \mathbb{C}^{n \times n}. \quad (6.7)$$

In Table 6.4 are shown the lowest eigenvalues with the aforementioned periodic boundary conditions for several values of the discretisation parameter and the exact values computed analytically.

| n | Eigenvalue | | | | | | | |
|-------|------------|---------|---------|---------|---------|---------|---------|---------|
| | 1 | 2 | 3 | 4 | 5 | 6 | 7 | 8 |
| 101 | -0.0000 | 39.4885 | 39.5103 | 39.5103 | 39.5487 | 79.0194 | 79.0643 | 79.0645 |
| 153 | 0.0000 | 39.4829 | 39.4923 | 39.4924 | 39.5094 | 78.9849 | 79.0043 | 79.0044 |
| 201 | -0.0000 | 39.4810 | 39.4865 | 39.4866 | 39.4965 | 78.9733 | 78.9845 | 78.9845 |
| 251 | 0.0000 | 39.4801 | 39.4836 | 39.4837 | 39.4900 | 78.9675 | 78.9746 | 78.9747 |
| Exact | 0.0 | 39.4784 | 39.4784 | 39.4784 | 39.4784 | 78.9568 | 78.9568 | 78.9568 |

Table 6.4: Eigenvalues for periodic boundary conditions for discretisation sizes $n = 101, 153, 201, 251$.

6.4. Quasiperiodic boundary conditions. In this example we show how to implement quasiperiodic boundary conditions (also called Bloch-periodic boundary conditions). We will consider a situation in which we impose quasiperiodic boundary conditions between the sides I_1 and I_3 of the previous example and periodic boundary conditions between I_2 and I_4 . The unitary operator that implements the exact boundary condition is

$$U = \begin{bmatrix} 0 & 0 & e^{i\alpha} T^* & 0 \\ 0 & T^* & 0 & 0 \\ e^{-i\alpha} T^* & 0 & 0 & 0 \\ 0 & 0 & 0 & T^* \end{bmatrix}, \quad (6.8)$$

where $e^{i\alpha}$ is the complex phase between the sites I_1 and I_3 , cf. [16, Example 5.3]. This is, it suffices to multiply by a complex phase and its conjugate the appropriate rows of the unitary operator implementing periodic boundary conditions defined in the previous example. Similar calculations to those in the previous example lead to the unitary matrix to be used as input in the problem

$$U = \begin{bmatrix} U_0 & 0 \\ 0 & -U_0 \end{bmatrix} \in \mathbb{C}^{8n \times 8n}, \quad U_0 = \begin{bmatrix} 0 & 0 & e^{i\alpha} P & 0 \\ 0 & P & 0 & 0 \\ e^{-i\alpha} P & 0 & 0 & 0 \\ 0 & 0 & 0 & P \end{bmatrix} \in \mathbb{C}^{4n \times 4n}, \quad P = \begin{bmatrix} 0 & & 1 \\ & \ddots & \\ 1 & & 0 \end{bmatrix} \in \mathbb{C}^{n \times n}. \quad (6.9)$$

In Table 6.5 are shown the lowest eigenvalues for the case $\alpha = \frac{\pi}{4}$ and the exact analytical values of the problem, which are given by the formula

$$E = 4\pi^2 \left(m^2 + \left(n + \frac{1}{8} \right)^2 \right), \quad m, n \in \mathbb{Z}.$$

One of the eigenfunctions is shown in Fig. 6.2.

| n | Eigenvalue | | | | | | | |
|-------|------------|---------|---------|---------|---------|---------|---------|---------|
| | 1 | 2 | 3 | 4 | 5 | 6 | 7 | 8 |
| 101 | 0.6173 | 30.2514 | 40.1278 | 40.1370 | 50.0140 | 69.7748 | 69.8242 | 89.5459 |
| 151 | 0.6170 | 30.2373 | 40.1099 | 40.1142 | 49.9870 | 69.7363 | 69.7584 | 89.5242 |
| 201 | 0.6170 | 30.2323 | 40.1036 | 40.1060 | 49.9774 | 69.7224 | 69.7349 | 89.4892 |
| 251 | 0.6169 | 30.2299 | 40.1006 | 40.1022 | 49.9730 | 69.7159 | 69.7239 | 89.4728 |
| Exact | 0.6168 | 30.2256 | 40.0952 | 40.0952 | 49.9648 | 69.7040 | 69.7040 | 89.4432 |

Table 6.5: Eigenvalues for quasi-periodic boundary conditions for $\alpha = \frac{\pi}{4}$ for discretisation sizes $n = 101, 151, 201, 251$.

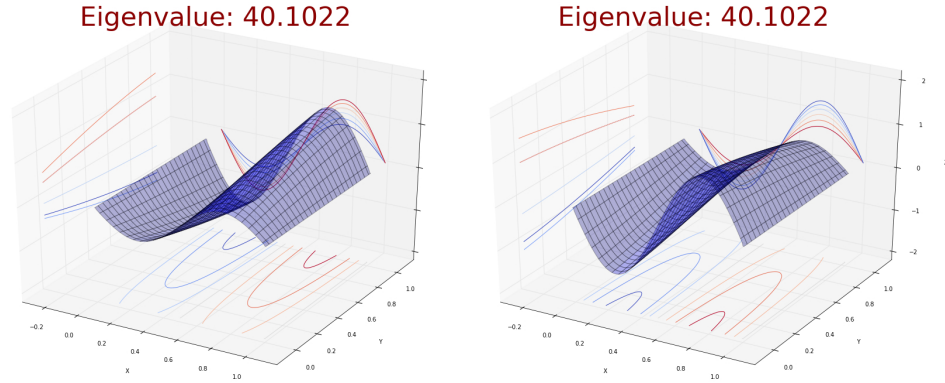


Fig. 6.2: Eigenfunction corresponding to the 4th eigenvalue for quasi-periodic boundary conditions with $\alpha = \frac{\pi}{4}$. Real and imaginary parts are plotted separately.

6.5. Discontinuous Robin boundary conditions. In this final example we will consider a situation with less trivial natural boundary conditions. We will consider piecewise constant Robin boundary conditions. These introduce discontinuities at the boundary at the points where the Robin parameter changes. The weak formulation of the Laplace operator presented here can handle with this singularities without special modifications as the analytical structure of the problem is well-defined even in this discontinuous situation.

The unitary operator in this case is almost identical to the one appearing in Section 6.2 with the exception that for half of the boundary we have to take a value of the Robin parameter Λ_1 different from the Robin parameter Λ_2 on the other half. The singularities are placed in the middle of the intervals I_2 and I_4 . In Table 6.6 the results for $\Lambda_1 = -\Lambda_2 = 1$ are shown.

| n | Eigenvalue | | | | | | | |
|-----|------------|--------|---------|---------|---------|---------|---------|---------|
| | 1 | 2 | 3 | 4 | 5 | 6 | 7 | 8 |
| 101 | -1.3236 | 7.8229 | 10.7855 | 22.5004 | 36.9358 | 42.5570 | 52.5901 | 54.2087 |
| 153 | -1.4483 | 7.5909 | 10.7521 | 22.4242 | 36.7601 | 42.3032 | 52.4507 | 53.7178 |
| 201 | -1.5149 | 7.4705 | 10.7339 | 22.3796 | 36.6794 | 42.1556 | 52.3795 | 53.4519 |
| 251 | -1.5621 | 7.3869 | 10.7208 | 22.3460 | 36.6276 | 42.0448 | 52.3294 | 53.2599 |
| 301 | -1.5966 | 7.3264 | 10.7110 | 22.3199 | 36.5923 | 41.9597 | 52.2925 | 53.1164 |
| 351 | -1.6233 | 7.2799 | 10.7034 | 22.2988 | 36.5664 | 41.8913 | 52.2636 | 53.0031 |
| 401 | -1.6448 | 7.2428 | 10.6972 | 22.2812 | 36.5465 | 41.8344 | 52.2400 | 52.9103 |

Table 6.6: Eigenvalues for discontinuous Robin boundary conditions for discretisation sizes $n = 101, 153, 201, 251, 301, 351, 401$.

Since the exact solution cannot be obtained analytically, we have computed the approximation of the same problem with the standard approach for natural boundary conditions. That is, we have taken the basis of the Neumann problem and have computed the contribution of the matrix F , Eq. (4.4), as

$$\langle \varphi(x), \Lambda(x)\varphi(x) \rangle.$$

Here, $\varphi(x)$ are the piecewise linear continuous functions that correspond to the restriction to the boundary of the Neumann boundary functions. The results are presented in Table 6.7.

| n | Eigenvalue | | | | | | | |
|-----|------------|--------|---------|---------|---------|---------|---------|---------|
| | 1 | 2 | 3 | 4 | 5 | 6 | 7 | 8 |
| 101 | -2.2909 | 6.2365 | 10.4792 | 21.4133 | 36.1646 | 39.2590 | 49.0981 | 51.3412 |
| 151 | -2.3361 | 6.1410 | 10.4683 | 21.4028 | 36.0637 | 39.2186 | 49.0288 | 51.3178 |
| 201 | -2.3597 | 6.0923 | 10.4630 | 21.3992 | 36.0152 | 39.2014 | 49.0008 | 51.3125 |
| 251 | -2.3742 | 6.0628 | 10.4598 | 21.3975 | 35.9867 | 39.1921 | 48.9861 | 51.3115 |
| 301 | -2.3840 | 6.0430 | 10.4576 | 21.3966 | 35.9680 | 39.1862 | 48.9772 | 51.3116 |
| 351 | -2.3911 | 6.0287 | 10.4561 | 21.3960 | 35.9549 | 39.1822 | 48.9713 | 51.3122 |
| 401 | -2.3964 | 6.0180 | 10.4549 | 21.3956 | 35.9450 | 39.1794 | 48.9671 | 51.3128 |

Table 6.7: Eigenvalues for discontinuous Robin boundary conditions for discretisation sizes $n = 101, 151, 201, 251, 301, 351, 401$ computed with the standard FEM for natural boundary conditions.

As it can be seen, both methods converge. In both cases, the convergence of the negative eigenvalues is slow as is to be expected. However, the results do not converge to the same values. Although the computations for the standard approach converge slightly faster, we believe that the results of our approach, showed in Table 6.6, are more trustable. In the algorithm introduced in this article, the boundary conditions are implemented exactly and the operator A_U^N is the operator A_U of the exact problem. Therefore, the convergence to the solutions of the exact problem is granted as shown in Section 3. On the contrary, using the standard approach to treat natural boundary conditions, the problem fails to be approximated exactly at the discontinuities. Indeed, at the discontinuities, the Robin parameter is approximated by a linear polynomial with slope $\frac{2}{h}$, being h the step of the discretisation. Hence, the function $\Lambda(x)$ does not converge in the Sobolev norm of order 1 to the exact Robin function. Of course, the situation treated here is known to be singular and there are known ways to choose the boundary element functions in order to improve

the standard approach, cf. [27] and references therein, as well as use mesh refinement around the discontinuity points. Our algorithm presents the advantage that it chooses implicitly appropriate base-functions at the boundary in the absence of an *a priori* estimation of the discretisation or of the finite element basis.

REFERENCES

- [1] R. ABRAHAM, J. MARSDEN, AND T. RATIU. *Manifolds, Tensor Analysis and Applications*. Springer, 1988.
- [2] R.A. ADAMS AND J.J.F. FOURNIER. *Sobolev Spaces*. Pure and Applied Mathematics. Academic Press, Oxford, second edition, 2003.
- [3] M. ASOREY, A.P. BALACHANDRAN AND J.M. PÉREZ-PARDO. *Edge states: Topological insulators, superconductors and QCD chiral bags*. JHEP **2013**, (12) 073 (2013).
- [4] M. ASOREY, A. IBORT, G. MARMO. *The topology and geometry of self-adjoint and elliptic boundary conditions for Dirac and Laplace operators*. Int. J. Geom. Methods in Modern Physics, **12** (6) 1561007 (2015).
- [5] I. BABUŠKA, F. NOBILE AND R. TEMPONE. *A stochastic Collocation method for elliptic partial differential equations with random input data* SIAM J. Num. Anal., **45** (3) 1005–1034 (2007).
- [6] I. BABUŠKA, J. OSBORN *Eigenvalue Problems* Handbook of numerical analysis, vol. II Elsevier, North-Holland, 1991.
- [7] I. BABUSKA AND M. SURI. *On locking and Robustness in the Finite Element Method*. SIAM J. Num. Anal., **29** 1261–1293 (1992).
- [8] I. BABUŠKA, R. TEMPONE AND G.E. ZOURARIS. *Galerkin finite Element Approximations of Stochastic Elliptic Partial Differential Equations*. SIAM J. Numer. Anal. **42**, 800–825 (2004).
- [9] I. BABUŠKA, R. TEMPONE AND G.E. ZOURARIS. *Solving elliptic boundary value problems with uncertain coefficients by the finite element method- the stochastic formulation*. Compt. Methods Appl. Mech. Engng. **194**, 1251–1294 (2005).
- [10] D. BOFFI. *Finite element approximation of eigenvalue problems*. Acta Numerica **19**, 1–120 (2010).
- [11] S.C. BRENNER AND L.R. SCOTT. *The Mathematical Theory of Finite Element Methods*. Springer, second edition, 2008.
- [12] E.B. DAVIES. *Spectral Theory and Differential Operators*. Cambridge University Press, 1995.
- [13] J.W. DEMMEL. *Applied Numerical Linear Algebra*. SIAM, 1997.
- [14] G. GRUBB *Krein-like extensions and the lower boundedness problem for elliptic operators*. J. Differential Equations **252**, 852–885 (2012).
- [15] A. IBORT, F. LLEDÓ, J.M. PÉREZ-PARDO. *On self-adjoint extensions and symmetries in quantum mechanics*. Annales Inst. Henri Poincaré, **16**, 2367–2397 (2014).
- [16] A. IBORT, F. LLEDÓ, AND J.M. PÉREZ-PARDO. *Self-adjoint extensions of the Laplace-Beltrami operator and unitaries at the boundary*. J. Funct. Analysis, **268** (3), 634–670 (2014).
- [17] A. IBORT, G. MARMO, J.M. PÉREZ-PARDO. *Boundary dynamics driven entanglement*. Journal of Physics A: Mathematical and Theoretical, **47** (38), 385301 (2014).
- [18] A. IBORT, J. M. PÉREZ-PARDO. *Numerical solutions of the spectral problem for arbitrary self-adjoint extensions of 1D Schrödinger equation*. SIAM J. Num. Anal., **51** (2) 1254–1279 (2013).
- [19] A. IBORT, J.M. PÉREZ-PARDO. *On the theory of self-adjoint extensions of symmetric operators and its applications to Quantum Physics*. Int. J. Geom. Methods in Modern Physics, **12** (6), 1560005 (2015).
- [20] T. KATO. *Perturbation Theory for Linear Operators*. Classics in Mathematics. Springer, 1995.
- [21] J.L. LIONS AND E. MAGENES. *Non-homogeneous Boundary Value Problems and Applications*, volume I of *Grundlehren der mathematischen Wissenschaften*. Springer, 1972.
- [22] J.M. PÉREZ-PARDO, M. BARBERO-LIÑÁN, A. IBORT. *Boundary dynamics and topology change in quantum mechanics*. Int. J. Geom. Methods in Modern Physics, **12**, 1560011 (2015).
- [23] R. RAM-MOHAN. *Finite Element and Boundary Element Applications in Quantum Mechanics*. Oxford University Press, 2002.
- [24] M. REED AND B. SIMON. *Methods of Modern Mathematical Physics*, volume I. Academic Press, New York and London, 1972.
- [25] M. REED AND B. SIMON. *Methods of Modern Mathematical Physics*, volume IV. Academic Press, New York and London, 1978.
- [26] K. SCHMÜDGEN. *Unbounded self-adjoint operators on Hilbert space*. Springer, Dordrecht, 2012.
- [27] T. STROUBOULIS, I. BABUSKA AND K. COPPS. *The design and analysis of the Generalised Finite Element Method*. Compt. Methods Appl. Mech. Engng. **181**, 43–69 (2000).
- [28] N. SUKUMAR AND J.E. PASK. *Classical and enriched finite element formulations for Bloch-periodic boundary conditions*. Int. J. Numer. Meth. Engng. **77**, 1121–1138 (2009).
- [29] M.E. TAYLOR. *Partial Differential Equations I*, volume 115 of *Applied Mathematical Sciences*. Springer, 1996.